Fuel 427 (2027) 139882

Contents lists available at ScienceDirect

Fuel

journal homepage: www.elsevier.com/locate/fuel

Full Length Article

Methane-fueled gas turbine with hydrogen blending and integrated steam Rankine cycle, absorption refrigeration cycle, PEM electrolyzer, and a CO_2 separation unit

Amr S. Abouzied [a], Hyder H. Abed Balla [b,*], Omar J. Alkhatib [c,*], Ahmed G. Abokhalil [d], Mahidzal Dahari [e,*], M.A. Ahmed [f,*], Zahra Bayhan [g], Dhaffaf Saud Alrasheed [h], Yasser Fouad [i,*], Ibrahim Mahariq [j,k,l,m,**]

[a] Department of Pharmaceutical Chemistry, College of Pharmacy, University of Hail, Hail 81442, Saudi Arabia
[b] Aeronautical Technical Department, Najaf Technical Institute, Al Furat Al Awsat Technical University, Iraq, Najaf, Kufa, Iraq
[c] Architectural Engineering Department, United Arab Emirates University, Al Ain, United Arab Emirates
[d] Sustainable and Renewable Energy Engineering Department, University of Sharjah, Sharjah, United Arab Emirates
[e] Deparment of Electrical Engineering, Faculty of Engineering, Universiti Malaya, 50603 Kuala Lumpur, Malaysia
[f] Department of Mathematics, College of Science, Majmaah University, Al-Majmaah 11952, Saudi Arabia
[g] Department of Physics, College of Sciences, Princess Nourah Bint Abdulrahman University, P.O. Box 84428, Riyadh, 11671, Saudi Arabia
[h] Computer & Information technology Department, Aljouf Technical College for Girls- Sakaka, Aljouf, Saudi Arabia
[i] Department of Applied Mechanical Engineering, College of Applied Engineering, Muzahimiyah Branch, King Saud University, P.O. Box 800, Riyadh 11421, Saudi Arabia
[j] College of Engineering and Architecture, Gulf University for Science and Technology, Mishref, Kuwait
[k] Department of Electrical and Electronic Engineering, Faculty of Engineering and Architecture, Istanbul Gelisim University, Avcılar- Istanbul, 34310, Istanbul, Turkiye
[l] Department of Medical Research, China Medical University Hospital, China Medical University, Taichung, Taiwan
[m] University College, Korea University, Seoul 02481, South Korea

ARTICLE INFO

Keywords:
Methane fuel
Hydrogen blending
Gas turbine
Multi-generation power system
Steam Rankine cycle
Genetic algorithm-based optimization

ABSTRACT

This research introduces and optimizes a novel multi-generation power system integrating a steam Rankine cycle (SRC), a gas turbine (GT), an absorption refrigeration cycle (ARC), a proton exchange membrane (PEM) electrolyzer, and a CO_2 separation unit. This system is designed to improve energy efficiency while simultaneously capturing CO_2 and producing hydrogen through electrolysis. Two configurations—with and without ARC—are evaluated using a genetic algorithm-based multi-objective optimization framework, which considers exergetic efficiency, CO_2 emission reduction, and total cost rate. The findings demonstrate that the proposed system improves exergetic efficiency by up to 71% and reduces CO_2 emissions by up to 3.9% compared to a standalone GT system. Furthermore, the system without ARC achieves higher hydrogen production, while the system with ARC provides valuable cooling. These findings demonstrate the feasibility and environmental advantages of integrated power, CO_2 capture, and H_2 blending systems for sustainable energy generation.

1. Introduction

The energy industry is facing increasing pressure to reduce greenhouse gas emissions while ensuring a secure, efficient, and cost-effective energy supply [1,2]. Fossil-fuel power plants, particularly gas turbines, remain a dominant source of electricity worldwide [3–5]. However, their continued operation poses serious environmental challenges due to high CO_2 emissions and heat losses [6,7]. To address these concerns, researchers and engineers have increasingly focused on integrating carbon capture technologies and heat recovery strategies into conventional power systems [8,9].

1.1. Literature review

The oxy-fuel combustion method, physical absorption techniques,

* Corresponding authors.
** Corresponding author at: University College, Korea University, Seoul 02481, South Korea.
E-mail addresses: hyderballa@atu.edu.iq (H.H. Abed Balla), omar.alkhatib@uaeu.ac.ae (O.J. Alkhatib), mahidzal@um.edu.my (M. Dahari), moh.hassan@mu.edu.sa (M.A. Ahmed), yfouad@ksu.edu.sa (Y. Fouad), mahariq@korea.ac.kr (I. Mahariq).

https://doi.org/10.1016/j.fuel.2026.139882
Received 12 December 2025; Received in revised form 7 April 2026; Accepted 9 May 2026
Available online 20 May 2026
0016-2361/

Nomenclature

Symbol	Description, Unit
A	Area, m^2
c	Unit cost, \$/kg or \$/kWh
C	Cost rate, \$/h
Cp	Specific heat capacity, kJ/kg·K
d	Distance to ideal point (LINMAP), –
D	Membrane thickness, Mm
ex	Specific exergy, kJ/kg
Ex	Exergy rate, kW
f	Objective function value, –
h	Specific enthalpy, kJ/kg
i	Interest rate, %
J	Current density, A/m
k	Component cost factor, –
LHV	Lower heating value, kJ/kg
m	Mass flow rate, kg/s
n	Project life, years
N	Operating hours per year, h
P	Pressure, kPa
Q	Heat transfer rate, kW
R	Gas constant, kJ/kg·K
s	Specific entropy, kJ/kg·K
T	Temperature, K or °C
v	Voltage, V
W	Work / Power, kW or MW
Y	Mole fraction, –
Z	Capital cost, \$

Greek Symbols

Δ	Variation/Difference, –
ε	Standard chemical exergy / Effectiveness, kJ/k mol
η	Efficiency, %
λ	Water content, –
σ	Ionic conductivity, S/m
ϕ	Maintenance factor, –
activ	Activation
ARC	Absorption Refrigeration Cycle
ch	Chemical
Comp	Compressor
Cond	Condenser
D	Destruction
elec	Electrical
en	Energy
env	Environmental
eva	Evaporator
ex	Exergy
GT	Gas Turbine
in	Inlet
LCOE	Levelized Cost of Electricity
LCOH	Levelized Cost of Hydrogen
out	Outlet
PEM	Proton Exchange Membrane
ph	Physical
RC/SRC	Rankine Cycle
SP	Solution Pump
T	Turbine
TEG	Thermoelectric Generator

adsorption techniques, and membrane technologies may all be used to capture CO_2 before and after combustion [10–13]. To have an insight into CO_2 and its future value chains, a comprehensive and comparative review by Jarvis et al. [14,15] can be helpful. In addition to discussing the pricing of CO_2 separation, transportation, and storage, the team examined and compared several CO_2 conversion technologies. Using a variety of technologies used in CO_2 capture, lifecycle environmental effects were also analyzed [16]. Ghiat et al. [17] have also reviewed the utilization and carbon capture in the energy, water, and food nexus systems. Recent advancements in multigeneration systems have explored diverse configurations to maximize energy recovery and system efficiency [11]. For instance, researchers have evaluated novel plants that combine cooling, power, and seawater desalination, using supercritical CO_2 partial cooling and absorption refrigeration cycles. Similarly, integrated systems combining supercritical CO_2 with gas turbines and organic Rankine cycles have been analyzed for waste-energy recuperation [14,18,19].

Gas turbines are commonly used in power plants and, in some cases, can be integrated with steam turbines. Typically, gas turbines are considered closed cycles for simulation [20]. Gaining a deeper understanding of the advancements and challenges in simulating gas-turbine power plants could be beneficial, as they provide most of the world's energy. In their study, Gonzalez et al. [21] thoroughly examined and categorized different techniques for CO_2 capture, focusing on the challenges and advantages specific to gas turbine power plants. Furthermore, gas turbines are frequently integrated with Rankine or organic Rankine cycles (ORCs), as demonstrated by Maheshwari et al. [22] in their research article. They compared different arrangements of combined power cycles that included GT, SRC, and ORCs. Their findings indicated a maximum work output of 638 kJ/kg when all three power units were combined. Additionally, the energy efficiency was calculated at 54.95%, while the exergy efficiency was 57.87%. Another innovative operating scenario for integrated gas-steam cycles was proposed by Zhong et al. [23]. Furthermore, research studies have explored the combination of micro gas turbines with SRCs, solar collectors, and/or ORCs [24], and even refrigeration cycles [6]. Lu et al. [25] executed a comprehensive dynamic thermal-supply model for a 2-by-1 combined cycle gas turbine and Rankine cycle. They designed a control system consisting of valves to maintain stable water levels during mode changes and investigated the impact of switching on the system's dynamic behavior [26,27].

To enhance efficiency, incorporating a refrigeration subsystem can establish a more effective, comprehensive multigenerational system called CCHP [28,29]. Three approaches are commonly employed to meet the cooling load requirements: the ejector refrigeration cycle [30–32], compression [33,34], and absorption chiller cycles [35]. Moghimi et al. [36] have extensively researched and evaluated these systems, investigating their thermodynamic performance from various perspectives, including energy, exergy, economics, and environmental considerations. In their study, they specifically focused on CCHP and the gas turbine ejector refrigeration cycle as the prime mover. Results indicated the integrated cycle achieved energetic and exergetic efficiencies that exceeded those of the Brayton cycle by 12% and 7%, respectively. Abbasi et al. [37] also conducted analyses encompassing energy, exergy, and economic evaluations of a CCHP system using a gas turbine and a gas engine. Integrating these primary movers, namely the gas turbine and diesel engine, led to an impressive 80% cost reduction, 62.8% exergy efficiency, and 87% energy efficiency. Likewise, Chen et al. [38] explored absorption chillers, proposing, designing, and optimizing a cascade refrigeration system with meticulous attention.

Thermoelectric generators are used to harness electricity from the surplus heat dissipated in an energy system [39]. However, their electricity output is comparatively low, posing limitations for grid integration. To effectively use the produced electricity, it is channeled towards the proton exchange membrane (PEM) electrolyzer, enabling the production of hydrogen and oxygen [40,41]. Subsequently, these products are extracted via the heat recovery process within a multigeneration framework that leverages the output power [42]. Furthermore, to mitigate the harmful impact of fossil fuels in gas turbines, a prevalent practice is to use hydrogen generated by PEM electrolyzers as a supplementary fuel for the combustors, a technique called hydrogen blending. Taamallah et al. [43] extensively investigated the stability and flexibility of fuel in gas turbines with hydrogen blending. An investigation into the numerical analysis of hydrogen-natural gas fuel blends for use in a microturbine's rich combustor was undertaken, leading to the development of an enhanced combustion chamber through the creation of a computational fluid dynamics (CFD) model with varying hydrogen fractions [44]. Ozturk and Dincer [45] analyzed the integration of binary and flash systems with a hydrogen production unit to blend the produced hydrogen with methane for daily applications.

For a well-designed integrated system to reduce practical expenses, environmental impacts, and improve thermodynamic performance, it is often necessary to optimize and arrange it in the best possible way. Putting in place a multigeneration power plant has multiple objectives, making the optimization process a multi-objective process [6,46–48].

1.2. Deficiencies

The literature reviewed contains outstanding ideas for multigeneration systems, heat recovery methods, and carbon capture techniques. However, some deficiencies or lack could be noted in the literature, some of which are listed in Table 1.

1.3. Main contributions

Despite extensive research on multigeneration energy systems, few studies have addressed the simultaneous integration of gas turbines, heat recovery systems, hydrogen production, and CO_2 capture within a unified, optimized framework. The present work addresses this critical gap by proposing a comprehensive system architecture and offering a robust optimization framework. The key contributions of this work are the following:

- **System Integration:**

A comprehensive, fully integrated multigeneration energy system is proposed combining absorption refrigeration cycle (ARC), gas turbine (GT), steam Rankine cycle (SRC) proton exchange membrane (PEM) electrolyzer, thermoelectric generator (TEG), and a CO_2 separation unit. This configuration enables simultaneous production of electricity, heating, cooling, and hydrogen while capturing a significant portion of the system's carbon emissions.

- **Scenario-Based Evaluation:**

Two operational scenarios are evaluated:

Scenario A: Without an absorption chiller, where recovered heat is utilized for direct heating.

Scenario B: With an absorption chiller, where recovered heat produces a cooling load.

This comparison reveals trade-offs between hydrogen production, thermal recovery, and cooling capacity.

- **Hydrogen Blending:**

Hydrogen produced by the PEM electrolyzer is blended with natural gas before combustion in the gas turbine. This approach reduces fossil fuel consumption and CO_2 emissions, contributing to fuel flexibility and system decarbonization.

- **Advanced CO_2 Separation:**

A membrane-based CO_2 separation unit is introduced and integrated with downstream heat exchange processes. A novel filtering mechanism is proposed to improve capture performance while maintaining system efficiency.

- **Multi-Objective Optimization Using Machine Learning:**

A multi-objective genetic algorithm (GA) is coupled with a neural network surrogate model to optimize key metrics—namely, CO_2 emission reduction, overall cost rate, and exergetic efficiency. The machine learning model accelerates convergence and enables deeper parametric analysis under a wide range of input conditions.

- **Comparative Benchmarking:**

The performance of the proposed system is benchmarked against both a conventional GT power plant and a CCHP system with absorption cooling. The comparison highlights superior exergy efficiency (up to 71%), higher hydrogen output, and CO_2 reduction by as much as 3.9%, depending on the configuration.

These contributions demonstrate the technical feasibility and ecological advantages of coupling electricity generating, hydrogen production, and CO_2 capture in a unified, optimized platform—marking a significant step toward net-zero power systems.

The research follows a systematic four-stage computational framework to evaluate and refine the proposed multigeneration system:

- Stage 1- Thermodynamic Modeling: A comprehensive mathematical model is developed and implemented in MATLAB to simulate the steady-state performance of the integrated Gas Turbine, Steam Rankine Cycle, PEM Electrolyzer, and CO_2 separation unit. The core

Table 1
Literature review concerned with the research scope.

References	Examinations Energy	Exergy	Economic	Environmental	Optimization	Multi-generation products Power	Cooling	Hydrogen	Hydrogen blending	CO_2 capture
[6]	✓	✓	✓	✓	*Yes*	✓	✓	–	–	✓
[22]	✓	✓	–	–	–	✓	–	–	–	–
[23]	✓	✓	–	–	–	✓	–	–	–	–
[36]	✓	✓	✓	✓	–	✓	✓	–	–	–
[37]	✓	✓	✓	–	–	✓	–	–	–	–
[49]	✓	✓	–	✓	–	✓	✓	✓	–	–
[50]	✓	–	✓	✓	–	✓	✓	–	–	✓
[51]	✓	–	✓	–	–	✓	–	–	–	✓
[52]	✓	✓	–	–	–	✓	–	✓	–	–
[53]	✓	–	✓	–	–	✓	–	–	–	✓
[54]	✓	✓	✓	✓	–	✓	–	–	–	–
[55]	✓	✓	✓	–	–	✓	–	–	–	✓
Present study	✓	✓	✓	✓	*Yes*	✓	✓	✓	✓	✓

of this model is built upon fundamental mass and energy conservation principles.

- Stage 2- 4E Analysis: The system is subjected to a rigorous 4E assessment, comprising Energy (first-law efficiency), Exergy (second-law destruction and efficiency), Economic (capital and operational cost rates), and Environmental (CO_2 emission reduction and carbon footprint) evaluations.
- Stage 3- Parametric Study: Key operational variables—including compressor pressure ratio, air mass flow rate, and turbine inlet pressure—are varied to observe their physical influence on system outputs such as Net Power, LCOE, and the CO_2 reduction index.
- Stage 4- Multi-Objective Optimization: To identify the optimal trade-off between competing goals, a multi-objective Genetic Algorithm (GA) is coupled with a neural network surrogate model. This final stage utilizes the LINMAP method to pinpoint the best operational point across three primary objective functions: exergetic efficiency, overall cost rate, and CO_2 emission reduction.

2. System description

The designed energy framework is a fully integrated multigeneration configuration intended to concurrently generate electricity, hydrogen, cooling, heating, and to capture CO_2 emissions. It combines a steam Rankine cycle (SRC), a proton exchange membrane (PEM) electrolyzer, a gas turbine (GT), an absorption refrigeration cycle (ARC), and a membrane-based CO_2 separation unit. The gas turbine operates functions on a blend of hydrogen and natural gas, generating electricity while releasing high-enthalpy exhaust gases. A heat recovery steam generator is the designated recipient of these exhaust gases, where they provide the thermal input to a bottoming SRC. The steam produced is expanded in a turbine in order to produce additional electricity, and the remaining heat in the condenser is further utilized depending on the operational scenario.

Two system configurations are considered: one without ARC, where the recovered heat is used for district or industrial heating (see Fig. 1(a)); and one with ARC, where the condenser heat drives an absorption chiller to produce a cooling load (see Fig. 1(b)). In both cases, a portion of the electricity generated is used to create a PEM electrolyzer to produce hydrogen and oxygen. The hydrogen is blended with natural gas and reinjected into the GT combustor, improving fuel flexibility and reducing CO_2 emissions. The oxygen is stored for potential external use. After passing through the thermal recovery stages, the flue gases are routed to a membrane-based CO_2 separation unit, where carbon is filtered prior to atmospheric release. To further maximize energy recovery, low-grade residual heat across the system is harvested using TEGs. This integrated design captures energy from multiple stages and forms, significantly improving system efficiency and sustainability compared to traditional power plants.

3. Mathematical modeling

The suggested framework is implemented using MATLAB and analyzed through mathematical formulations. The core framework encompasses a thermodynamic analysis, an economic evaluation, and an environmental assessment. The associated mathematical expressions are derived from principles of mass and energy conservation and foundational economic and environmental theories. This part outlines the employed mathematical expressions in detail. To construct the framework, several assumptions and prerequisites are essential:

- The system operates in a steady state mode.
- The dead state conditions are 101.325 kPa and 25 °C.
- Pressure drops by 0.02% of the inlet pressure in the combustion chamber.
- Pressure drops by 0.05% of the inlet pressure in all heat exchangers.
- The combustion process is considered complete.

3.1. Thermodynamic model

The fundamental thermodynamic formulas applied in this research are the equations of energy balance and exergy balance, as presented below [6].

$$\dot{Q} + \sum \dot{m}_{in}\ (h_{in} - h_0) = \dot{W} + \sum \dot{m}_{out}\ (h_{out} - h_0) \tag{1}$$

$$\sum \left(1 - \frac{T_0}{T_{source}}\right)\dot{Q}_{source} - \dot{W} + \sum \dot{m}_{in}\ ex_{in} - \sum \dot{m}_{out}\ ex_{out} = \dot{E}x_D \tag{2}$$

whereby, ex is the specific exergy (kJ/kg), and $\dot{E}x$ represents exergy rate (kW). T_0 and T_{source} denote ambient temperature and heat source temperature (K), respectively. Index D in Eq. (2) represents the destruction of exergy.

Exergy possesses an absolute value, distinguishing it from energy, which is inherently a relative measure. Exergy can exist in various forms, such as potential, kinetic, physical, and chemical. In the current model, changes in gravitational potential and significant variations in kinetic energy are absent, rendering kinetic and potential exergies insignificant. Thus, the definition of specific exergy is as follows [56]:

$$ex = ex^{ch} + ex^{ph} \tag{3}$$

where, ex^{ch} and ex^{ph} are chemical and physical exergies, respectively, and can be articulated as follows [56]:

$$ex^{ph} = C_p\left(T - T_0 - T_0\ln\left(\frac{T}{T_0}\right)\right) + RT_0\ln\left(\frac{P}{P_0}\right) \tag{4}$$

$$ex^{ch} = n\left(\sum_i y_i\varepsilon_i + \overline{R}T_0\sum_i y_i\ln(y_i)\right) \tag{5}$$

where, C_p is specific heat capacity (kJ/kg. K). R represents the gas constant (kJ/kg K). n is the number of moles, mole fraction is represented by y_i, and ε_i (kJ/k mole) is standard chemical exergy for i^{th} component.

Energy and exergy efficiencies are determined by the ratio of the desired output to the necessary input, as expressed below [6]:

$$\eta_{en} = \frac{\sum \dot{W}_{electricity} + \dot{Q}_{eva} + \dot{m}_{H_2} \times LHV_{H_2}}{\dot{m}_{fuel} \times LHV_{fuel}} \times 100 \tag{6}$$

$$\eta_{ex} = \frac{\sum \dot{E}x_{out}}{\sum \dot{E}x_{in}} \times 100 = \frac{\dot{E}x_{\dot{Q}_{eva}} + \sum \dot{W}_{electricity} + \dot{E}x_{H_2}}{\dot{m}_{fuel} \times LHV_{fuel}} \times 100 \tag{7}$$

where $\sum \dot{W}_{electricity}$ is the net generated electricity (kW). $\dot{Q}_{eva}$ (kW) is the amount cooling load generated in the absorption chiller, while $\dot{E}x_{\dot{Q}_{eva}}$ (kW) are the and exergy of this cooling load, respectively. LHV_{H_2}, $\dot{E}x_{H_2}$, and $\dot{E}x_{fuel}$ are the low heat value (LHV) of hydrogen (kJ/kg), exergy rate of hydrogen stream (kW), and exergy of fuel (kW), respectively.

This study involves multiple subsystems, each characterized by its unique modeling approach. The mathematical formulations for the membrane-based separator, gas turbine system, absorption chiller cycle (ACC), Rankine cycle, and PEM electrolyzer are outlined sequentially below.

Thermodynamics First and Second Law's Equations.

The exergy and energy formulas for GT, SRC, and ARC cycles are given in Table 2.

PEM electrolyzer.

Hydrogen production through a PEM electrolyzer (PEME), which operates by dissociating the molecules of water, is an efficient and versatile approach for energy storage and various applications. To optimize the efficacy of the hydrogen-energy cycle, the generated hydrogen is utilized within the facility as fuel, thereby minimizing CO_2

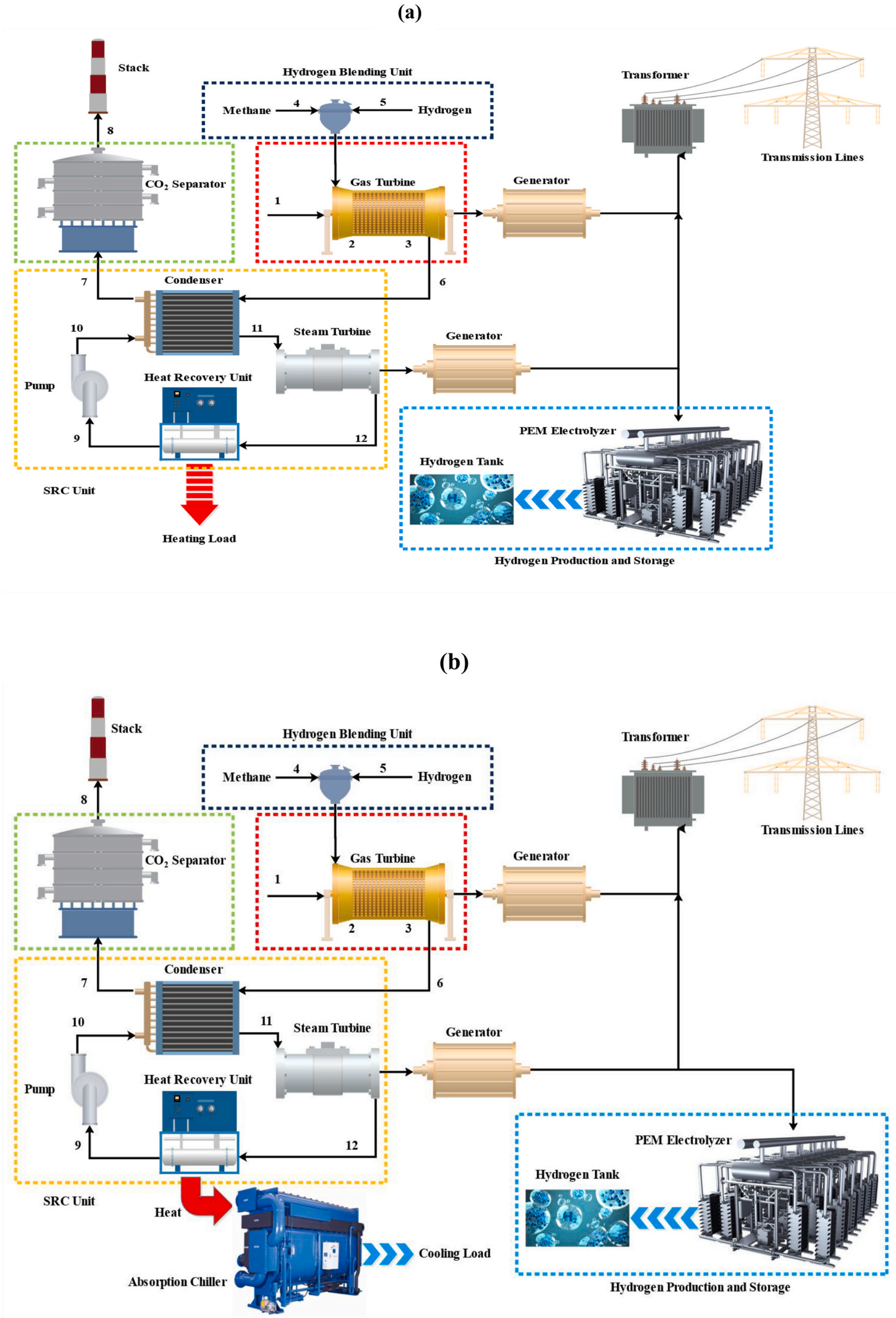

Fig. 1. (a) PFD of the system without absorption chiller subsystem (b) PFD of the system with absorption chiller subsystem.

Table 2
Energy and exergy balance equations for gas turbine [6,37].

Component	Energy balance equations	Exergy destruction rate equations
Air compressor	$\dot{W}_{Comp} = \dot{m}_{air}(h_{CD} - h_{CS})$	$\dot{E}x_{D,Comp} = \dot{E}x_{CS} + \dot{W}_{Comp} - \dot{E}x_{CD}$
Combustion chamber	$\dot{m}_{fuel}LHV + \dot{m}_{air}h_{TI} = \dot{m}_{TI}h_{TI}$	$\dot{E}x_{D,CC} = \dot{E}x_{CD} + \dot{m}_{fuel}ex^{0}_{ch,fuel} - \dot{E}x_{TI}$
Gas turbine	$\dot{W}_{GT} = \dot{m}_{TI}(h_{TI} - h_{TE})$ $\dot{m}_{TI} = \dot{m}_{fuel} + \dot{m}_{air}$	$\dot{E}x_{D,GT} = \dot{E}x_{TI} - \dot{E}x_{TE} - \dot{W}_{GT}$
Heat exchanger/SRC Evaporator	$\dot{m}_{TI}(h_{HEI} - h_{HEE}) = \dot{m}_{SRC}C_{Eva}(h_{Eva,out} - h_{Eva,in})$	$\dot{E}x_{D,HEX1} = \dot{E}x_{HEI} + \dot{E}x_{Eva,in} - \dot{E}x_{Eva,out} - \dot{E}x_{HEE}$
SRC turbine	$\dot{W}_{SRCT} = \dot{m}_{SRC}(h_{SRCT,in} - h_{SRCT,out})\eta_{SRCT} = (h_{SRCT,in} - h_{SRCT,out})/(h_{SRCT,in} - h_{SRCT,out,s})$	$\dot{E}x_{D,SRCT} = \dot{E}x_{SRCT,in} - \dot{W}_{SRCT} - \dot{E}x_{SRCT,out}$
SRC condenser	$Q_{Cond,SRC} = \dot{m}_{SRC}(h_{Cond,SRC,in} - h_{Cond,SRC,out})$	$\dot{E}x_{D,Cond,ORC} = \dot{E}x_{Cond,SRC,in} + \dot{E}x_{Q_{Cond,SRC}} - \dot{E}x_{Cond,SRC,out}$
SRC pump	$\dot{W}_{SRCP} = \dot{m}_{SRC}(h_{SRCP,out} - h_{SRCP,in})\eta_{SRCP} = (h_{SRCP,out,s} - h_{SRCP,in})/(h_{SRCP,out} - h_{SRCP,in})$	$\dot{E}x_{D,SRCP} = \dot{E}x_{SRCP,in} + \dot{W}_{SRCP} - \dot{E}x_{SRCP,out}$
Steam generator	$Q_{SG} = \dot{m}_{WS}h_{WS} + \dot{m}_{R}h_{R} - \dot{m}_{SS}h_{SS}$	$\dot{E}x_{D,SG} = \dot{E}x_{SS} + \dot{E}x_{Q_{SG}} - \dot{E}x_{R} - \dot{E}x_{WS}$
Absorber	$\dot{Q}_{Abs} = \dot{m}_{WS}h_{WS} + \dot{m}_{R}h_{R} - \dot{m}_{SS}h_{SS}$	$\dot{E}x_{D,Abs} = \dot{E}x_{WS} + \dot{E}x_{R} - \dot{E}x_{SS}$
ARC condenser	$Q_{Cond} = \dot{m}_{R}(h_{Cond,in} - h_{Cond,out})$	$\dot{E}x_{D,ARC,cond} = \dot{E}x_{ARC,Cond,in} + Q_{ARC,Cond} - \dot{E}x_{ARC,Cond,out}$
ARC evaporator	$\dot{Q}_{ARC,Eva} = \dot{m}_{R}(h_{Eva,out} - h_{Eva,in})$	$\dot{E}x_{D,\mathrm{ARC,Eva}} = \dot{E}x_{Q_{Eva}} + \dot{E}x_{ARC,Eva,in} - \dot{E}x_{ARC,Eva,out}$
Refrigerant expansion valve	$h_{in} = h_{out}$	$\dot{E}x_{D,REV} = \dot{E}x_{ARC,REV,in} - \dot{E}x_{ARC,REV,out}$
Solution expansion valve	$h_{in} = h_{out}$	$\dot{E}x_{D,SEV} = \dot{E}x_{ARC,SEV,in} - \dot{E}x_{ARC,SEV,out}$
Solution pump	$\dot{W}_{SP} = \dot{m}_{SS}(h_{out} - h_{in})\eta_{SP} = v_{in}(P_{out} - P_{in})/(h_{out} - h_{in})$	$\dot{E}x_{D,SP} = \dot{E}x_{ARC,SP,in} + \dot{W}_{SP} - \dot{E}x_{ARC,SP,out}$

emissions and transportation expenses. The performance of the PEME is described using governing equations, with its fixed parameters detailed in Tables 3 and 4.

3.2. Advanced CO_2 separation unit

The integrated framework utilizes a membrane-based separation unit designed for post-combustion carbon capture. Unlike conventional amine scrubbing, which incurs a high thermal penalty, this advanced unit employs a multi-stage polymeric membrane system characterized by high CO_2/N_2 selectivity.

- Operational Mechanism: The flue gas, after exiting the Heat Recovery Unit at a stabilized temperature (Middle Temperature), enters the separator where a partial pressure gradient drives the CO_2 through the membrane.
- Novel Filtering Mechanism: To maintain high capture efficiency without compromising the Gas Turbine's backpressure, the unit utilizes a "sweep gas" or vacuum-assisted permeate stream, which significantly lowers the energy required for compression.
- System Integration: The unit is strategically positioned after the Rankine cycle evaporator to ensure the gas is at an optimal thermal state for membrane permeability.

Table 4
Input parameters for the PEM electrolyzer [57].

Parameters	Value	Unit
Current density	A/m^2	5100
$\boldsymbol{T_{PEM}}$	K	353
$\boldsymbol{E_{act,a}}$	kJ/mol	76
$\boldsymbol{E_{act,c}}$	kJ/mol	18
$\boldsymbol{\lambda_a}$	–	14
$\boldsymbol{\lambda_c}$	–	10
D	μm	50
$\boldsymbol{J_a^{ref}}$	A/m^2	2×10^5
$\boldsymbol{J_c^{ref}}$	A/m^2	4.6×10^3

- Performance Metrics: This configuration allows the system to capture approximately one-third of the total CO_2 produced, directly contributing to the 3.9% net emission reduction observed in Scenario A.

Integration of CO_2 Separation and GT Performance.
A critical design feature of the proposed system is the strategic placement of the membrane-based CO_2 separation unit to minimize any "energy penalty" on the Gas Turbine (GT). In traditional carbon capture systems, diverting high-pressure or high-temperature gas can

Table 3
Electrochemical equations governing the PEME [57,58].

Parameter	Description	Governing equations
Theoretical energy for hydrogen generation	$T\Delta S$ indicates the thermal energy demand and ΔG is the electrical energy request.	$\Delta H = \Delta G + T\Delta S$
The electrical energy input for the electrolyzer	V and J are electrolyzers' voltage and current density.	$E_{elec} = JV$
Electrolyzer voltage	V_{ohm} denotes electrolyte's ohmic overpotential. V_0 indicates the reversible potential. $V_{activ,a}$ and $V_{activ,c}$ are anode activation overpotential and cathode activation overpotential, correspondingly.	$V = V_0 + V_{ohm} + V_{activ,a} + V_{activ,c}$
Ohmic overpotential	Based on the ohmic law	$V_{ohm} = JR_{PEM}$
Nernst equation	T_{PEM} is the temperature of the electrolyzer	$V_0 = 1.229 - 8.5 \times 10^{-4}(T_{PEM} - 298)$
The exchange current density of electrolysis	J_i^{ref} denotes the pre-exponential factor and $E_{act,i}$ denotes the activation energy.	$J_{0,i} = J_i^{ref} exp\left(-\frac{E_{activ,i}}{RT}\right) i = a,c$
Activation overpotential	c and a refer to anode and cathode, respectively.	$V_{activ,i} = \frac{RT}{F} sinh^{-1}\left(\frac{J}{2 \times J_{0,i}}\right) i = a,c$
Overall ohmic resistance	x denotes the distance within the membrane measured from the cathode membrane interface, while D represents the membrane thickness.	$R_{PEM} = \int_0^D \frac{dx}{\sigma[\lambda(x)]}$
Water content at a location x within the membrane	λ_c and λ_a represent the water contents at the cathode membrane and the anode membrane interfaces, correspondingly.	$\lambda(x) = \lambda_c + \frac{\lambda_a - \lambda_c}{D} x$
Local ionic conductivity	T is the membrane's temperature	$\sigma[\lambda(x)] = [0.5139\lambda(x) - 0.326]exp\left[1268\left(\frac{1}{303} - \frac{1}{T}\right)\right]$

significantly reduce the turbine's net output work. However, in this architecture, the separator is integrated as the final stage of the flue gas path.

The exhaust gases first expand completely in the gas turbine to produce electricity, then pass through the Heat Recovery Steam Generator (HRSG) to drive the Rankine cycle, and finally reach the separator. By the time the flue gas reaches the CO_2 separation unit, its thermal energy has already been harvested for power and for heating and cooling loads.

Furthermore, the pressure drop across the membrane unit is maintained at a very low level—modeled at 0.05% of the inlet pressure—preventing significant backpressure on the GT. This allows the system to achieve a CO_2 reduction of up to 3.9% without compromising the isentropic efficiency or the 35.5 MW net power output of the primary gas turbine cycle.

3.3. Econo-Environmental model

This study focuses on minimizing the carbon footprint while enhancing the overall system efficiency, with careful attention to economic factors. Economic assessments are grounded in the capital costs of individual components, operational and maintenance expenses, and variable costs like fuel input costs. Component prices can be fixed values in US dollars or expressed as cost functions dependent on operating parameters. The cost functions for equipment within each subsystem are detailed in Table 5 along with originating year of functions and their corresponding cost index. After setting a reference year, Equation (8) brings the cost functions up to date with the present year. Additionally, the cost functions, along with constant parameters and assumptions of the economic model, are summarized in Table 6 [6,59].

Table 6
Constant parameters of economic modeling [6].

Parameter	Value	Unit
n	20	Number of years
N	8000	Number of hours
Φ	1.06	Dimensionless
i	12	%
c_{fuel}	0.3456	\$/kg
$c_{electricity}$	0.161	\$/kWh

$$\dot{C}_{\text{total, cost}} = \sum_k \dot{Z}_k + \dot{C}_f + \dot{C}_{env} \tag{11}$$

where c_f denotes the mass unit price of the fuel (\$/kg); $\dot{m}_{fuel}$ denotes the inlet fuel flow rate. Also, c_{CO_2} represents the punishment cost for a mass unit of CO_2 production (\$/kg).

To evaluate the financial benefits of manufacturing diverse products (including electrical power and hydrogen), one can utilize the concept of levelized cost. Considering the production potential of different products as well as the corresponding units cost allows us to calculate the levelized cost of various products, as expressed by the two formulas that follow:

$$LCOE = \frac{\dot{Z}_{GT} + \dot{Z}_{RC} + \dot{Z}_{ORC}}{\dot{W}_{net,\ total}} \tag{12}$$

$$LCOH = \frac{(LCOE \times \dot{W}_{Elec}) + \dot{Z}_{PEME}}{\dot{m}_{H_2}} \tag{13}$$

where $\dot{W}_{Elec}$ is delivered value of electricity to PEM.

The economic feasibility of the integrated multigeneration system is

$$Cost\ at\ the\ year\ 2025 = Original\ cost \times \left(\frac{Cost\ index\ for\ the\ year\ 2025}{Cost\ index\ for\ the\ year\ when\ the\ original\ cost\ was\ obtained}\right) \tag{8}$$

The overall cost rate ($\dot{C}_{\text{total, cost}}$) is computed by aggregating the fuel cost rate ($\dot{C}_f$), the expense of each component ($\sum_k \dot{Z}_k$), and the environmental penalty associated with CO_2 emission into the atmosphere ($\dot{C}_{env}$) [37]:

$$\dot{C}_f = c_f \times \dot{m}_{fuel} \times 3600 \tag{9}$$

$$\dot{C}_{env} = c_{CO_2} \times \dot{m}_{CO_2} \times 3600 \tag{10}$$

Table 5
Cost functions of each component of the subsystems [6].

Equipment	Cost function (\$)	Original year – CEPCI index	Reference
Gas turbine package	11,000,000	1994 – 368.1	[37]
Heat exchanger	$Z_{HX1} = 2143 \times (A)_{HX1}^{0.514}$	1994 – 368.1	[60]
Absorption chiller	$Z = 1144.3 \times (Q_{eva})^{0.67}$	2015 – 556.8	[37]
SRC pump	$Z_{\mathrm{ORC,P}} = 200(\dot{W}_{\mathrm{P}})^{0.65}$	2003 – 402	[61]
SRC condenser	$Z_{\mathrm{ORC,Con}} = 516.62(A_{\mathrm{Eva}})^{0.6}$	2010 – 550.8	[61]
SRC turbine	$Z_{\mathrm{ORC,}} = 4750(\dot{W}_{\mathrm{T}})^{0.75}$	2003 – 402	[61]
Separator	50A	2015 – 556.8	[62–64]
PEME	$Z_{PEM} = 1000\dot{W}_{PEM}$	*2012——523*	[67]

evaluated using a Total Capital Recovery (TCR) approach based on the following assumptions and sources:

- Capital Costs (Z_k): The investment costs for major components, including the gas turbine, steam turbine, and heat exchangers, are derived from established cost functions indexed to the year 2025 using the Chemical Engineering Plant Cost Index (CEPCI).
- Fuel and Electricity Pricing: The mass unit price for methane (c_{fuel}) is set at 0.3456 \$/kg, while the benchmark for electricity ($c_{electricity}$) is 0.161 \$/kWh, reflecting average industrial rates.
- Environmental Penalties: A carbon tax or "punishment cost" (c_{CO_2}) is integrated into the overall cost rate to quantify the economic benefit of the membrane separation unit and hydrogen blending.
- Financial Parameters: The economic model assumes a project life (n) of 20 years, an annual operating time (N) of 8000 h, and an interest rate (i) of 12%.
- Maintenance and Operation: A dimensionless maintenance factor (φ) of 1.06 is applied to the total capital cost to account for ongoing operational expenses.

By aggregating these factors, the model calculates the Levelized Cost of Electricity (LCOE) and Hydrogen (LCOH), providing a realistic estimate of the system's commercial viability.

3.4. Optimization procedure

Optimization plays a crucial role in improving system performance, reducing resource consumption, and enabling more efficient and sustainable solutions across engineering and scientific applications [65,66]. The mathematical model is utilized to calculate the system's key outputs, though not all of these are treated as objectives. The most critical outputs—total exergy efficiency, overall cost rate, and CO_2 emission reduction—are objective functions. Designing a system to operate under optimal conditions is essential in engineering, particularly in energy systems. Therefore, an optimization process is necessary to determine the ideal input parameters and outputs, providing engineers with a rationale for implementing such projects. The optimization approach is inspired by natural processes, such as genetic algorithms (GA), which aim to minimize the objective functions. Since genetic algorithms are rooted in evolutionary theory, the objective function values in the final generation are expected to be optimized. The optimization process was conducted using the GA toolbox in MATLAB software under specific assumptions and conditions outlined below as provided in Table 7.

This study's objective functions are the hydrogen generation rate, total cost rate, and overall exergy efficiency. A genetic algorithm is employed for optimizing these objectives. The optimal solution, representing the most favorable values of the defined objective functions, will be identified utilizing the LINMAP method. LINMAP operates by calculating based on the objective functions' normalized results. The procedure includes calculating the normalized functions and determining the optimal point for assessment. The steps of this process are demonstrated below [61,67]:

$$f_{i,j}^{\star} = \frac{f_{i,j}}{\sqrt{\sum_{i=1}^{N}\left(f_{i,j}\right)^2}}, j = 1, 2, 3 \tag{13}$$

$$d_i = \sqrt{\sum_{j=1}^{3}\left(f_{i,j}^{*} - f_{\text{ideal}\ ,j}^{*}\right)^2} \tag{14}$$

where $f_{\text{ideal},j}^{*}$ and $f_{i,j}^{\star}$ denote ideal value and normalized value of each objective function, respectively. Also, the minimum distance between ideal values and optimal values of objective functions is determined by d_i.

3.5. Model assumptions and practical limitations

While the mathematical framework provides a robust basis for system evaluation, it is constructed under specific idealized conditions to ensure computational tractability. The following implications of these assumptions are acknowledged:

Table 7
Optimization parameters and assumptions.

Parameter	Values / Features
Training data numbers	600
Test data numbers	200
Validation data numbers	200
Hidden layers numbers	3
Hidden neurons numbers	4
Maximum iteration	10,000
Initial bias and weights	Random values
Validation checks	10
Learning method	Levenberg-Marquardt Back Propagation
Activation function	LogSigmoid (Hidden) and linear transfer function (Output)

- Steady-State Operation: The system is modeled in a steady state, which does not account for transient behaviors during startup, shutdown, or rapid load fluctuations common in grid-interactive settings.
- Neglect of Friction and Pressure Losses: Although fixed percentage pressure drops are integrated into the combustion chamber (0.02%) and heat exchangers (0.05%), localized friction losses and complex fluid-dynamic variations are simplified.
- Ideal Heat Transfer: Variations in heat transfer efficiency due to fouling, scaling, or environmental changes are not considered, potentially leading to an overestimation of thermal recovery in the Rankine and absorption cycles.
- Material Aging and Degradation: The model does not incorporate performance degradation over time, such as membrane fouling in the CO_2 separator or catalyst deactivation in the PEM electrolyzer.
- Combustion Efficiency: The assumption of complete combustion provides an upper bound for energy output and CO_2 generation, though actual turbine operations may involve trace incomplete combustion products.

These assumptions are justifiable for a preliminary feasibility and optimization study; however, they may result in minor discrepancies compared to real-world industrial applications. Future research will focus on dynamic simulations and experimental validation to bridge the gap between this theoretical architecture and practical implementation.

4. Results and discussion

In the following section, we examine how each decision variable influences the model's outputs. Before this analysis, the model's solver, implemented as a MATLAB programming function, is verified against established and reliable studies for validation.

4.1. Model validation

The model solver generates multiple key outputs and independent variables. The core subsystems are validated using distinct functions that demonstrate the model's accuracy. Fig. 2 illustrates the validation of the ARC (a) and PEME (b) subsystems, with results clearly indicating strong agreement with established studies. Following this, the programming scripts for each subsystem are combined to assess the primary outputs of the complete system. The resulting integrated, floating code can be applied to the full system or individual subsystems.

Since the entire system is new and cannot be found in similar studies, each subsystem is compared to the results of a valid study for validating the programming code. Gas turbine and RC subsystems have also been validated with similar studies in Table 8. All the errors for all subsystems are less than 10%, which is justifiable in engineering problems. So, the validated code is used for the entire system in different input conditions.

4.2. Parametric study

The validated model is employed to perform a parametric analysis by varying individual design parameters while holding all other inputs constant. Fig. 3 presents the influence of varying the mass flow rate of inlet air to the compressor on several key system outputs, including total net power, exergy efficiency, heating/cooling loads, levelized cost of electricity (LCOE), levelized cost of hydrogen (LCOH), and the CO_2 reduction index, under both operational scenarios.

As the compressor's inlet mass flow rate increases, the demand for fuel rises proportionally to maintain the energy balance in the combustion chamber. This yields an increased output of power from gas turbine along with the downstream Rankine cycle, thereby increasing the system's total net power generation. However, since both input and output exergy scale proportionally with the increased flow rate, the overall exergy efficiency remains nearly constant across the tested

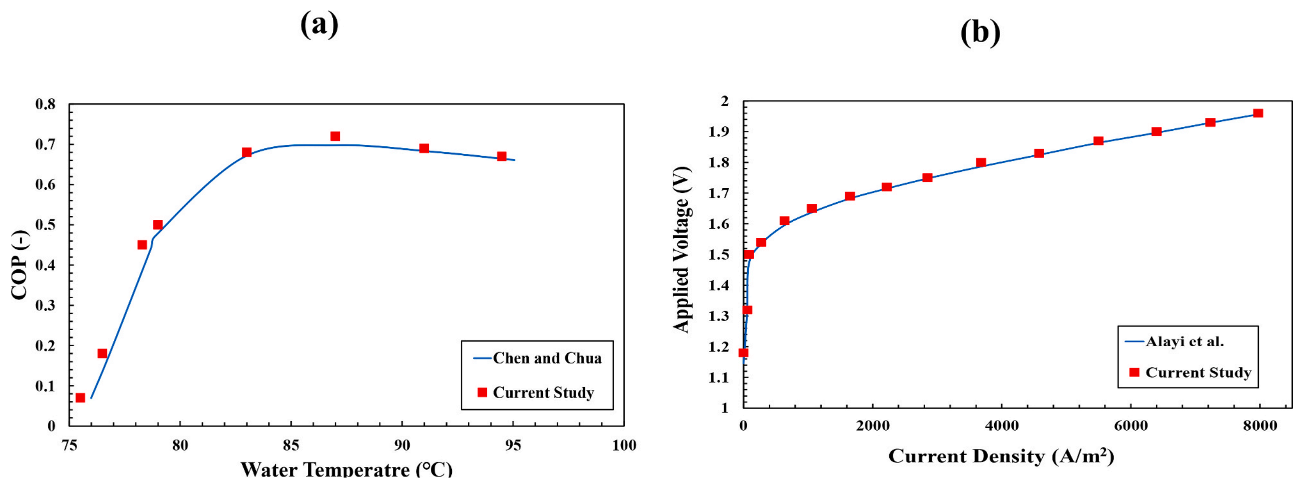

Fig. 2. Model validation for three main subsystems. Validation for (a) absorption chiller [38] and (b) PEM electrolyzer.

Table 8
Results of validation for RC and GT subsystems.

RC	**Parameter**	**Yari** [68]	**Current study**	**Error (%)**
	η_{ex}(%)	49.06	49.76	1.41
	Power (kJ/kg)	50.38	50.6	0.43
GT	**Parameter**	**Moghimi et al.** [36]	**Current study**	**Error (%)**
	η_{ex}(%)	32	33.12	3.5
	Power (MW)	37.25	37.92	1.77

range. In Scenario B (with ARC), the additional power also increases the electricity provided for the PEM electrolyzer, enhancing the rate of hydrogen generation. Moreover, the augmented waste heat availability supports a higher cooling load in the absorption refrigeration cycle.

The linear increase in net electricity and thermal loads with rising air mass flow rate is fundamentally driven by the working fluid's increased energy density. As the compressor processes a greater mass of air, the total enthalpy of the fluid entering the combustion chamber increases, requiring a proportional rise in fuel input to reach the target turbine inlet temperature. This results in a higher expansion work potential in the gas turbine and a greater availability of high-enthalpy exhaust gases for the downstream Heat Recovery Steam Generator (HRSG). The stability of the overall exergy efficiency, despite these gains, occurs because the exergy of the increased fuel and air inputs scales at the same rate as the produced power and chemical exergy of the hydrogen.

Fig. 4 illustrates the impact of varying the pressure ratio of compressor on key system operational indicators, with the upper panels representing Scenario A (without ARC) and the lower panels corresponding to Scenario B (with ARC). Increasing the pressure ratio results in enhanced isentropic efficiency during the compression process, which improves the thermal efficiency of the Brayton cycle and, consequently, enhances total net power output. As a result, the system's total exergetic efficiency increases as the pressure ratio rises.

However, as more energy is extracted in the high-pressure gas turbine stage, less thermal energy is available downstream for the absorption refrigeration cycle (ARC) and the steam Rankine cycle (SRC). This reduction in waste heat leads to a decline in both heating load (Scenario A) and cooling load (Scenario B). At the same time, reduced availability of electricity to the PEM electrolyzer results in a drop in hydrogen production, particularly in the high-pressure regime. Notably, the rate of hydrogen reduction surpasses the marginal savings in fuel consumption, resulting in an elevation of the levelized cost of hydrogen (LCOH).

Increasing the compressor pressure ratio enhances the isentropic efficiency of the Brayton cycle by expanding the temperature differential across which the gas turbine operates, leading to the observed rise in net electrical output and exergetic efficiency. Physically, however, this higher expansion in the turbine results in a lower turbine outlet temperature (TOT). This "thermal depletion" of the exhaust gas reduces the quality of the heat available to the bottoming Steam Rankine Cycle (SRC) and the Absorption Refrigeration Cycle (ARC), resulting in a precipitous drop in heating and cooling loads. Furthermore, the reduction in hydrogen production at higher pressures is due to diminished thermal energy recovery in the SRC, which limits the surplus electricity available to the PEM electrolyzer.

The effect of the steam Rankine cycle (SRC) turbine inlet pressure on the system's primary performance metrics is illustrated in Fig. 5 under both operational scenarios. In Scenario A (without ARC), increasing the turbine inlet pressure leads to a reduction in the mass flow rate through the SRC due to thermodynamic constraints, which slightly decreases the turbine's power output. However, this increase in inlet pressure enhances the temperature gradient across the condenser, enabling more effective heat recovery. As a result, additional electricity is made available to the PEM electrolyzer, increasing the hydrogen generation rate and reducing the levelized cost of hydrogen (LCOH).

The higher hydrogen yield enriches the fuel blend supplied to the gas turbine, displacing a portion of the methane and leading to a corresponding reduction in CO_2 emissions. This reduction contributes positively to the CO_2 mitigation index. Moreover, since exergy output is partially attributed to hydrogen production and, in Scenario B, to cooling load as well, the system exhibits an enhancement in exergy efficiency despite a marginal reduction in net generated electricity in Scenario A.

In Scenario B (with ARC), a similar trend is observed in hydrogen production; however, the gains in cooling capacity from the ARC are modest compared to the drop in net power output. Consequently, the improvement in overall exergy efficiency is limited, and in some cases, offset entirely. The LCOE experiences a mild reduction in both scenarios due to marginal shifts in power output and fuel demands. Overall, these results emphasize the importance of turbine inlet pressure as a critical control variable, particularly in balancing hydrogen output, exergy efficiency, and fuel substitution effects within the integrated system.

The increase in hydrogen production and CO_2 reduction with increasing SRC turbine inlet pressure is driven by improved thermal-to-electric conversion efficiency in the Rankine cycle. Higher inlet pressures increase the enthalpy drop across the steam turbine and, more importantly, optimize the temperature gradient within the condenser. This enables more effective low-grade heat recovery, resulting in increased power supply to the PEM electrolyzer. The subsequent rise in the hydrogen-to-methane ratio increases the chemical exergy of the fuel blend, displacing carbon-heavy methane and leading to the observed

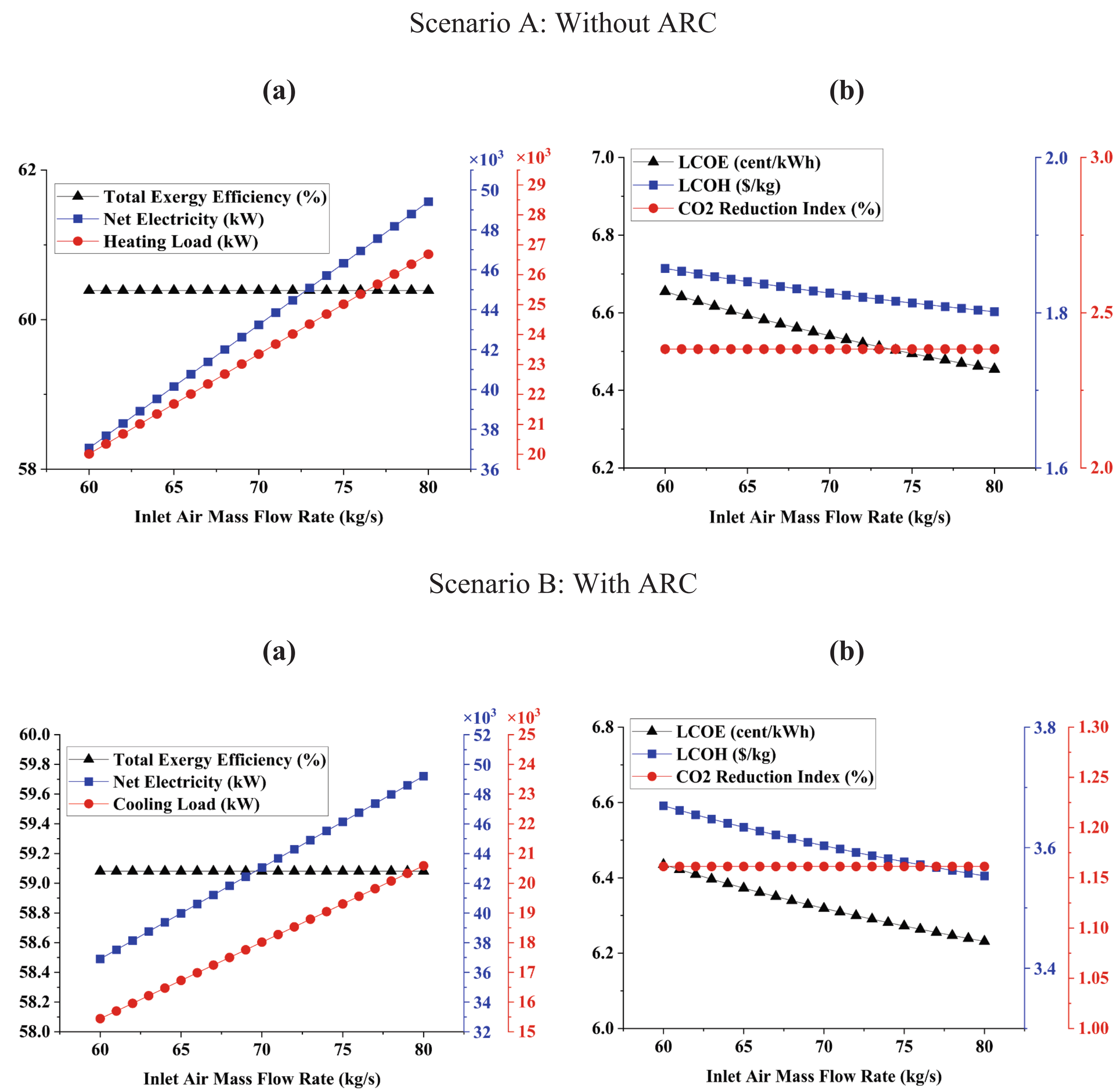

Fig. 3. The impact of compressor inlet air mass flow rate on the system's performance.

improvement in the CO_2 mitigation index.

Fig. 6 presents the effect of the temperature differential between the CO_2 separation unit and the heat exchanger on key system outputs. This temperature difference is a critical control parameter that reflects the thermal driving force available for heat recovery in the Rankine cycle (RC) and is influenced by factors such as heat exchanger effectiveness, flue gas flow rate, and constraints on turbine outlet temperature. In this analysis, the differential temperature was adjusted from 130 °C to 170 °C to evaluate the impact on system performance.

As the temperature differential increases, a smaller fraction of thermal energy is extracted by the RC, resulting in reduced steam generation and, consequently, a decline in power output from the RC turbine. This degradation in energy recovery directly reduces the total net power output of the system. In Scenario B (with ARC), the lower heat recovery also limits the thermal energy available to drive the absorption refrigeration cycle, leading to a decrease in cooling capacity. Simultaneously, less electricity is provided for the PEM electrolyzer, reducing hydrogen output and increasing the levelized cost of hydrogen (LCOH). These combined effects contribute to a measurable decline in exergy efficiency, as both power and hydrogen outputs diminish while input exergy remains largely unchanged.

The temperature differential across the heat exchanger-separator interface serves as a proxy for the system's "thermal dead weight". A higher differential indicates that a significant portion of the exhaust gas's thermal energy is bypassing the recovery stages and being released into the atmosphere or the CO_2 separation unit prematurely. This lack of effective heat exchange reduces the steam generation rate in the SRC, which cascades throughout the system, decreasing both turbine power and the energy available to the ARC and PEM subsystems. The resulting decline in exergy efficiency and the rise in LCOE are physical consequences of increased entropy generation in the heat-exchange process, where the driving force (temperature difference) is not effectively utilized for work.

Beyond steady-state performance, the system's controllability under part-load operation is a critical factor for grid integration. In scenarios where power demand fluctuates, the GT would likely serve as the primary control element, with the bottoming SRC and PEM electrolyzer adjusting their throughput accordingly. However, maintaining high exergetic efficiency at part load remains a challenge, as reduced mass flow rates can lead to off-design performance in heat exchangers and in

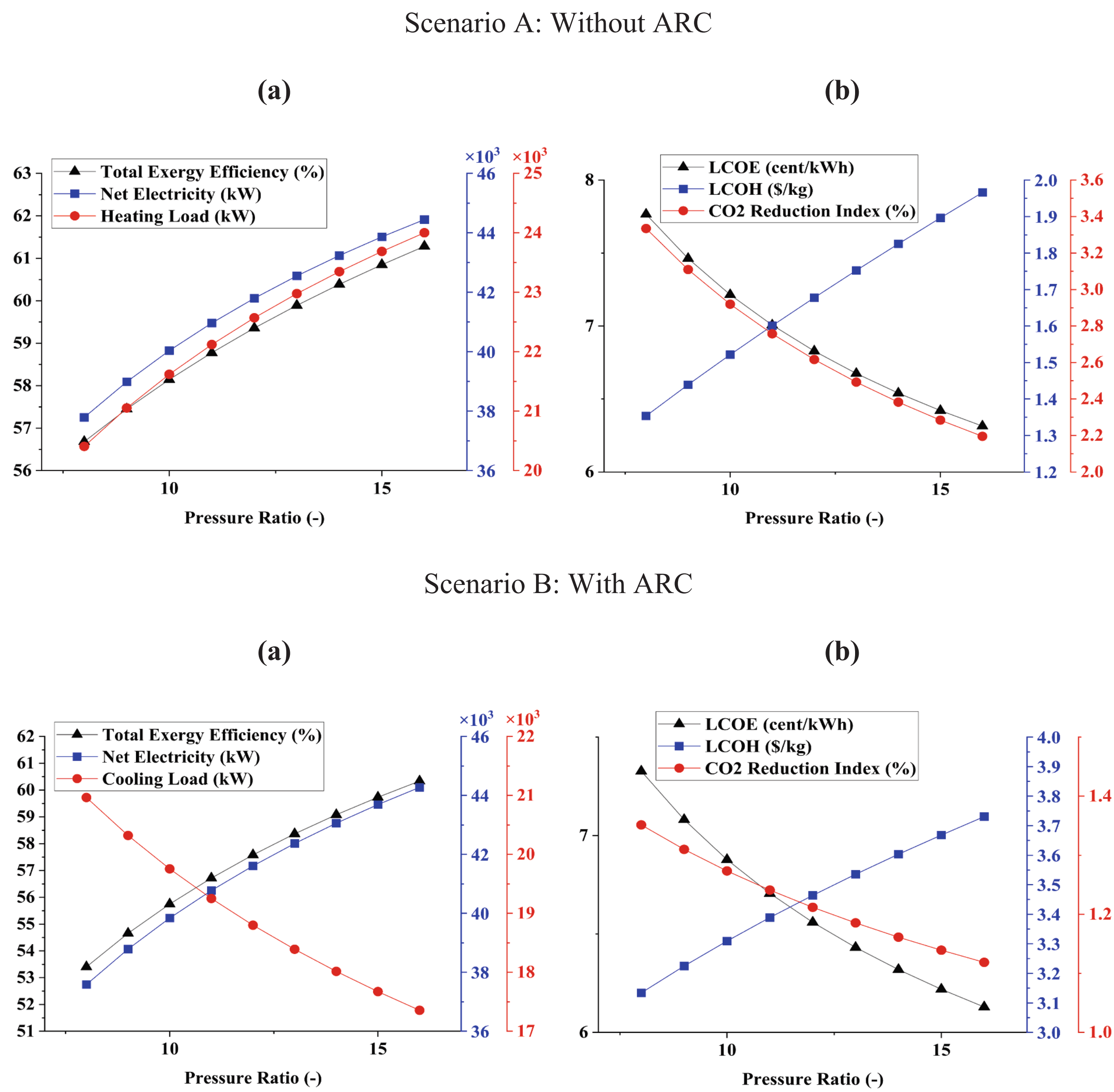

Fig. 4. The impact of compressor pressure ratio on the system's outputs.

the absorption refrigeration cycle.

Potential challenges and limitations include the high capital cost of the PEM electrolyzer and the complexity of managing a hydrogen-methane fuel blend with varying compositions. Additionally, the membrane-based CO_2 separator requires precise thermal management to avoid performance degradation. Future research should explore dynamic simulation models to evaluate transient response times and the integration of advanced control systems—such as model predictive control (MPC)—to stabilize the multigeneration outputs during variable load conditions.

4.3. Economic feasibility and practical implications

The economic viability of the proposed integrated system is evaluated through the lens of the Levelized Cost of Electricity (LCOE) and the Levelized Cost of Hydrogen (LCOH), alongside the total cost rate. At the optimal point for Scenario B (with ARC), the LCOE was 6.9 cents/kWh, which remains competitive with current global benchmarks for integrated gas-steam power plants. Conversely, Scenario A (without ARC) yields a higher LCOE of 8 cents/kWh due to the shift in energy allocation toward heating and enhanced hydrogen production. The cost of hydrogen production (LCOH) presents a significant trade-off between the two scenarios. In Scenario A, the LCOH is optimized at $1.8/kg, benefiting from higher hydrogen yields (150 kg/h) and a superior hydrogen-to-methane blending ratio of 0.068. This value aligns with the targets for “green” and “blue” hydrogen production costs required for industrial-scale adoption. In contrast, the ARC-equipped scenario results in an LCOH of $3.5/kg. While this is higher, it is offset by the generation of 18,000 kW of cooling load, which provides an additional revenue stream and utility in tropical or industrial cooling applications. Practical economic feasibility is further enhanced by the CO_2 separation unit. While the unit adds to capital expenditure ($50 per unit area), it significantly reduces environmental penalty costs (c_{CO_2}). The results indicate that integrating hydrogen blending with carbon capture can reduce the net carbon footprint by over 60% compared to standalone gas turbine systems. These findings suggest that while the initial investment for such a complex multigeneration plant is higher than traditional systems, the long-term economic benefits—driven by fuel savings from hydrogen blending, carbon tax mitigation, and the sale of multiple energy streams—support its implementation in decarbonizing power

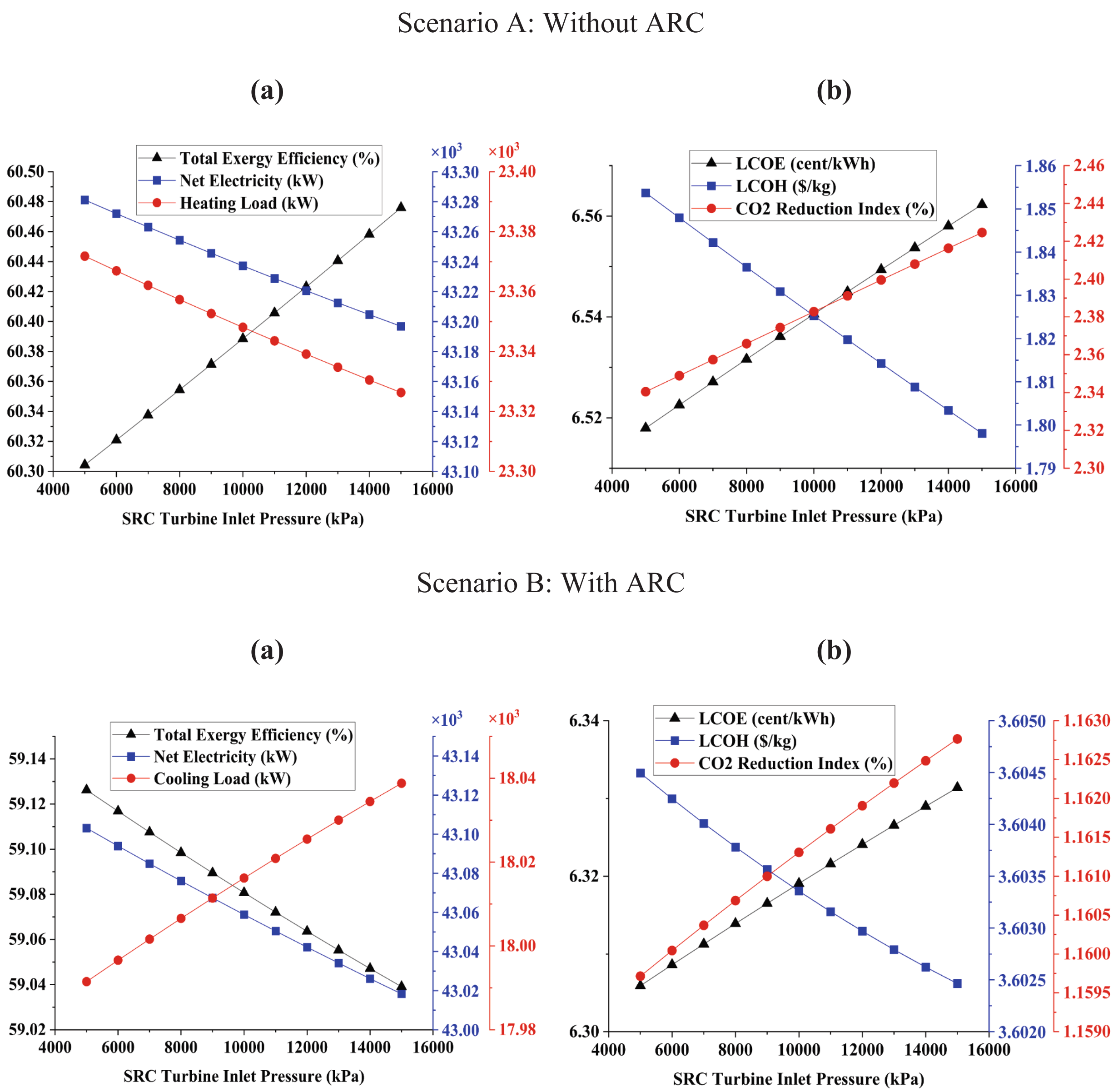

Fig. 5. The impact of the inlet pressure of the RC turbine on the main outputs of the system.

sectors.

4.4. Optimization results

A multi-objective optimization process was undertaken to identify the optimal functionality of the framework across three key objectives: overall exergy efficiency, total cost rate, and CO_2 reduction. Also, decision variables are: the inlet pressure of the RC turbine, the pressure ratio in the GT compressor, the air mass flow rate, and the middle temperature. Constraints in this problem include material limitations on high-temperature resistance, challenges in matching the working pressure/temperature of the steam turbine to those of the steam generator, and limitations on the air-to-fuel ratio in the combustion chamber. This analysis encompassed both operational scenarios to assess the system's behavior comprehensively. The optimization algorithm employed was Genetic Algorithm (GA) with an iterative approach until the predefined convergence criteria (tolerance of 10^{-4}) were satisfied. Also, the mutation and crossover fractions are 0.2 and 0.8, respectively. Convergence was achieved after 100 generations, indicating the algorithm had stabilized and identified a satisfactory solution space. The final generation comprised a population of 300 gene solutions. Each gene within this population was characterized by 105 distinct values for each objective function (exergy efficiency, cost rate, and CO_2 reduction) and 105 corresponding values for each decision variable. This representation captures a diverse set of potential operating points, allowing for a thorough exploration of the Pareto front and identifying trade-offs between the competing objectives.

Utilizing the LINMAP method [37], the best/optimal point was calculated among these 105 points for all objective functions and the corresponding values for decision variables. Fig. 7 (a) displays the three-dimensional Pareto frontier diagram for the scenario without ARC, while Fig. 7 (b) illustrates the Pareto frontier diagram for Scenario B, which includes ARC. These diagrams present four subplots: the top left indicates the three-dimensional representation, the top right showcases the overall cost rate in relation to exergetic efficiency, the bottom left displays the exergetic efficiency against CO_2 reduction, and the bottom right displays the total cost rate versus CO_2 reduction.

Table 9 presents the optimal decision variables and main outputs and compares the two scenarios. In the scenario with ARC, the system's mass flow is slightly higher than in the scenario without ARC. Additionally,

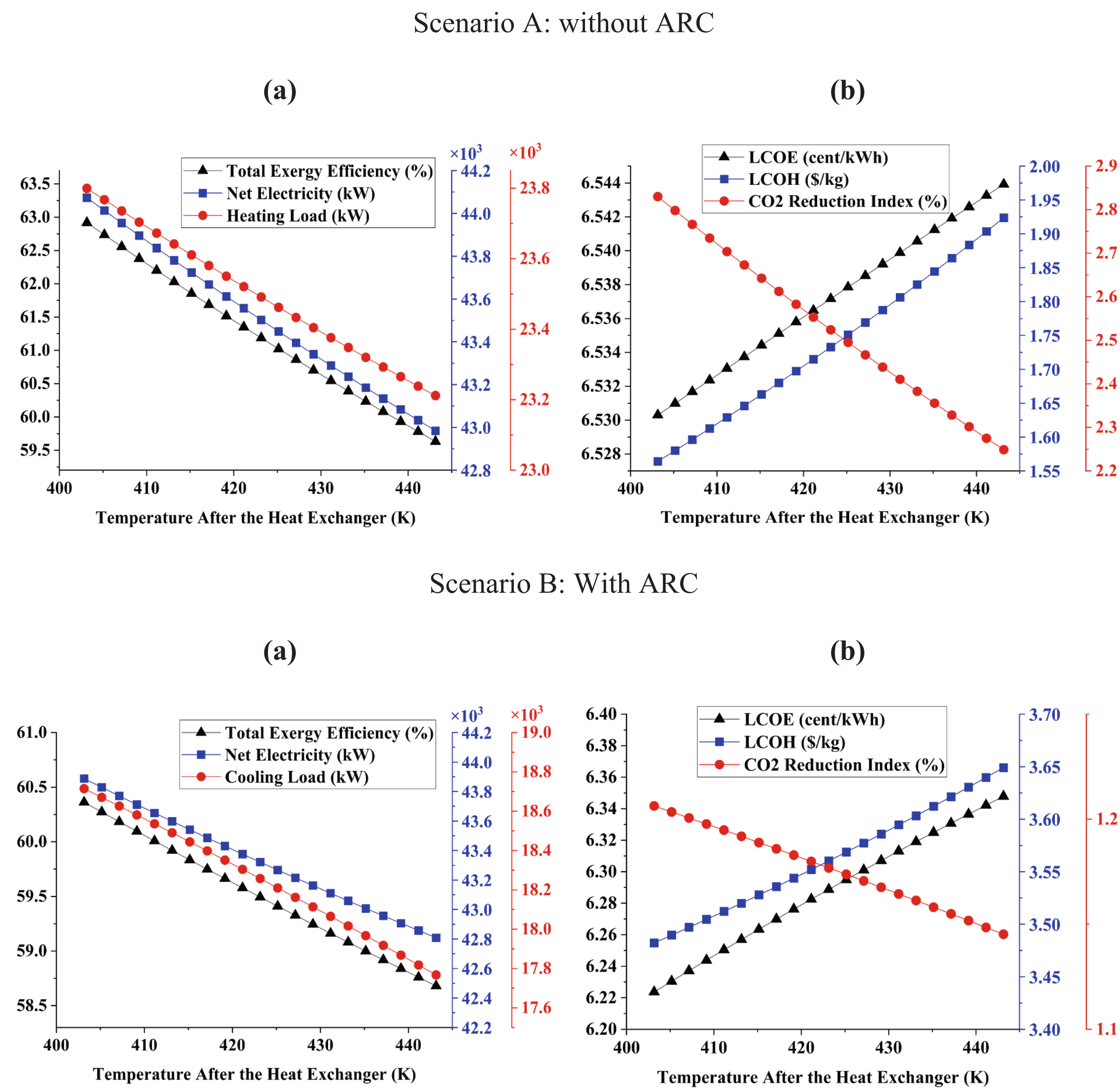

Fig. 6. Impact of the temperature between the heat exchanger and the separator on the system's primary outputs.

the compressor pressure ratio in the ARC scenario is 9.4, greater than in the scenario without ARC. In the case of ARC, the effectiveness, pressure inlet in the SRC turbine, and mid-temperature values are also higher.

Both scenarios demonstrate similar net output power and net income. However, the scenario with ARC generates a cooling load, whereas the scenario without ARC does not. Conversely, more hydrogen is produced in the scenario without ARC, resulting in a significantly higher hydrogen-to-methane ratio than the ARC scenario. The produced hydrogen in the scenario without ARC possesses substantial exergy, resulting in a significantly higher exergy efficiency and CO_2 reduction percentage than compared to the ARC scenario. However, the overall cost rate for the scenario without ARC surpasses that of the scenario with ARC.

Table 9 also includes the reported LCOE and LCOH values. The scenario with ARC requires fewer dollars for electricity production than without ARC. Conversely, less money is needed for hydrogen production in the scenario without ARC.

A comparative assessment of the two operational scenarios reveals a clear thermodynamic and economic trade-off between chemical energy production and thermal utility. In Scenario A, prioritizing heating results in a higher hydrogen production rate of 150 kg/h and a hydrogen-to-methane blending ratio of 0.068, significantly increasing the system's exergy efficiency to 71%. Conversely, integrating the ARC in Scenario B shifts energy allocation to provide a substantial 18,000 kW of cooling capacity. This shift, however, results in a reduction of the hydrogen-to-methane ratio to 0.013 and a lower exergetic efficiency of 56%. Economically, while Scenario B offers a more competitive LCOE of 6.9 cents/kWh, the LCOH rises to $3.5/kg, nearly double the $1.8/kg achieved in Scenario A. These results indicate that the system's configuration should be selected based on whether the primary objective is deep decarbonization via hydrogen or meeting high-demand industrial cooling requirements.

Fig. 8 visually represents the population distribution in the final generation of the optimization process for the ARC-less scenario. This figure substantially illustrates the focal point of optimization for each decision variable, highlighting the concentration of most of the population.

Fig. 9 compares outcomes between the two scenarios and a single gas turbine power plant, using the following baseline: a single gas turbine is assumed to operate under the same conditions as the current

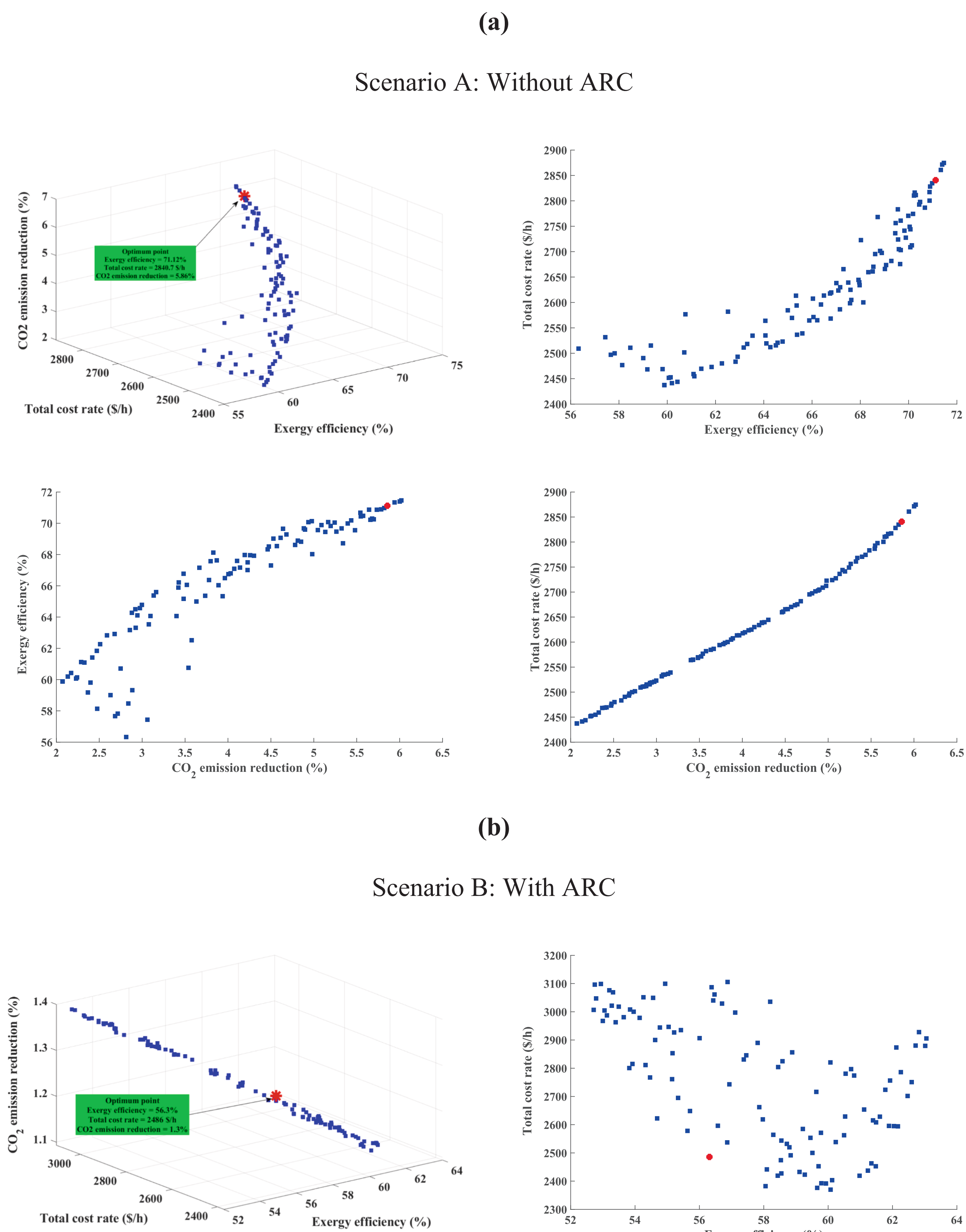

Fig. 7. (a) Pareto frontier results for Scenario A (without ARC). (b) Pareto frontier results for scenario B (with ARC).

unoptimized system, including inlet air and pressure ratio. It illustrates that the single power plant emits more CO_2 than in these scenarios due to their carbon capture and hydrogen blending methods. The separator captures and stores approximately one-third of the amount of CO_2 being produced. Hydrogen blending can directly affect the amount of CO_2 produced due to less fossil fuel consumption.

As depicted in Fig. 9, the system without ARC performs best, generating more power and achieving much higher exergy efficiency than the two cases at the optimum point. Its CO_2 emissions are lower than those of the GT power plant without a separation unit, and the

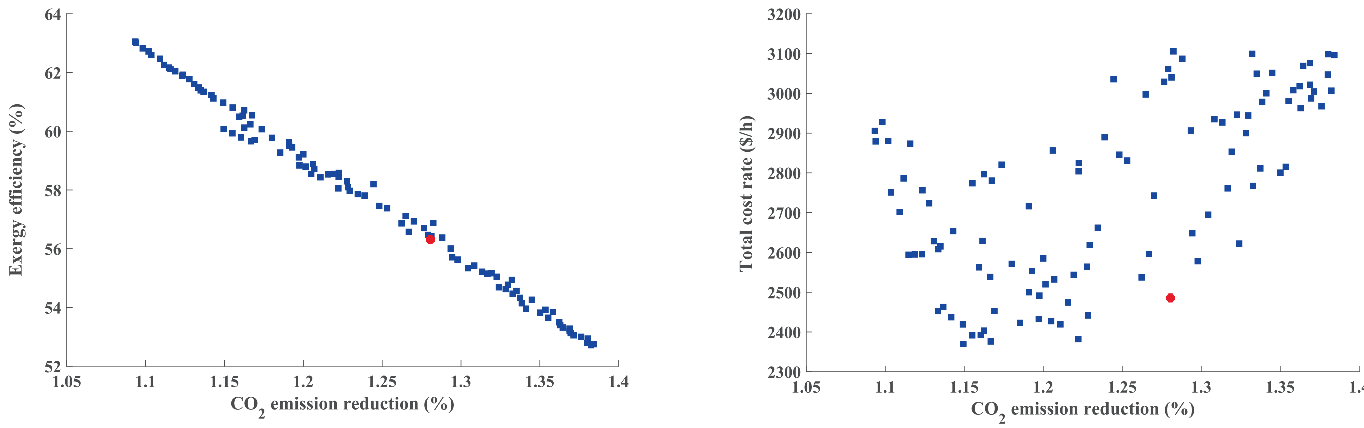

Fig. 7. (*continued*).

Table 9
Optimization results.

Parameter Optimum Design Parameters	Value Scenario With ARC	Scenario without ARC
RC's turbine inlet pressure (kPa)	7000	6000
Compressor pressure ratio	9.5	9
Air mass flow rate (kg/s)	62.5	60
Middle temperature (K)	418.5	403.5
System performance		
Total net power (kW)	35,887	35,483
Hydrogen to methane ratio (–)	0.013	0.068
Cooling load (kW)	18,000	–
Heating Load (kW)	–	24,000
Hydrogen production rate (kg/h)	160	150
LCOE (cent/kWh)	6.9	8
LCOH ($/kg)	3.5	1.8
Objective functions		
CO_2 emission reduction (%)	1.4	3.9
Overall cost rate ($/h)	2486	2845
Exergy efficiency (%)	56	71

system with ARC has a lower emission rate due to the hydrogen generation rate. However, the cost rate at the system's optimum point without ARC is slightly higher due to higher fuel consumption. To have a better view of exergy destruction, Table 10 has been provided.

While Scenario A is limited to providing a heating load of 24,000 kW, the transition to Scenario B allows the plant to meet high-demand refrigeration or air-conditioning requirements in industrial or tropical settings. Although this integration results in a slight reduction in the hydrogen-to-methane blending ratio (0.013 compared to 0.068 in Scenario A), it offers a critical functional benefit for multi-generational applications where cooling is a primary utility. This trade-off is further reflected in the exergetic efficiency, which remains high at 56% for the ARC-enabled configuration.

The performance of the proposed integrated system demonstrates a significant advancement over conventional and previously studied configurations. While standalone gas turbine (GT) systems typically achieve exergetic efficiencies of 32% to 33%, the current framework achieves superior efficiencies of 71% in Scenario A and 56% in Scenario B. This improvement is primarily attributed to the synergistic integration of the Steam Rankine Cycle (SRC), PEM electrolyzer, and thermoelectric generators (TEGs) for cascading waste heat recovery.

Compared to recent studies on CCHP systems that achieved exergy efficiencies of approximately 57.87%, our architecture provides a more versatile output stream by incorporating hydrogen blending and membrane-based CO_2 separation. Specifically, the ability to reduce CO_2 emissions by up to 3.9% while simultaneously producing 150 kg/h of hydrogen at a levelized cost of 1.8 $/kg highlights the environmental and economic competitiveness of this design. Unlike prior works that focused on single-utility recovery, this study offers a modular solution that balances high-grade power generation with diverse thermal and chemical products, marking a significant contribution toward the development of net-zero distributed energy systems.

The development and optimization of this multigeneration framework posed several technical challenges, particularly in integrating subsystems with vastly different operating regimes. Balancing the high-pressure requirements of the gas turbine with the low-grade heat recovery needs of the absorption refrigeration cycle and the PEM electrolyzer required precise thermal matching to avoid excessive entropy generation. Additionally, modeling the membrane-based CO_2 separation unit downstream of the recovery stages involved managing low-pressure flue gases while maintaining high capture selectivity.

Despite these hurdles, the study highlights several innovative methods:

- **Integrated 4E-GA Framework:** The use of a multi-objective GA coupled with a neural network surrogate model allowed for the simultaneous optimization of energy, exergy, economic, and environmental metrics, significantly accelerating convergence compared to traditional iterative methods.
- **Synergistic Hydrogen Blending:** Unlike conventional carbon capture studies, this work utilizes hydrogen produced on-site to enrich the methane fuel, achieving a dual benefit of lower carbon intensity at the source and post-combustion capture at the stack.
- **Scenario-Based Versatility:** The methodological approach of comparing "Heating-Hydrogen" (Scenario A) and "Cooling-Hydrogen" (Scenario B) configurations provides a novel decision-making roadmap for tailoring multigeneration plants to specific regional climate demands.

4.5. Analysis of CO_2 reduction sources

The total CO_2 reduction achieved by the integrated system is a cumulative result of two distinct mechanisms: pre-combustion fuel substitution and post-combustion carbon capture. At the optimal operating point (Scenario A), the system achieves a total CO_2 reduction of 3.9%. This reduction is broken down as follows:

- **Hydrogen Blending (Fuel Substitution):** By utilizing the PEM electrolyzer to produce hydrogen, which is then blended with methane at a ratio of 0.068, a portion of the fossil fuel input is directly displaced. This reduces the combustion process's carbon intensity at the source.

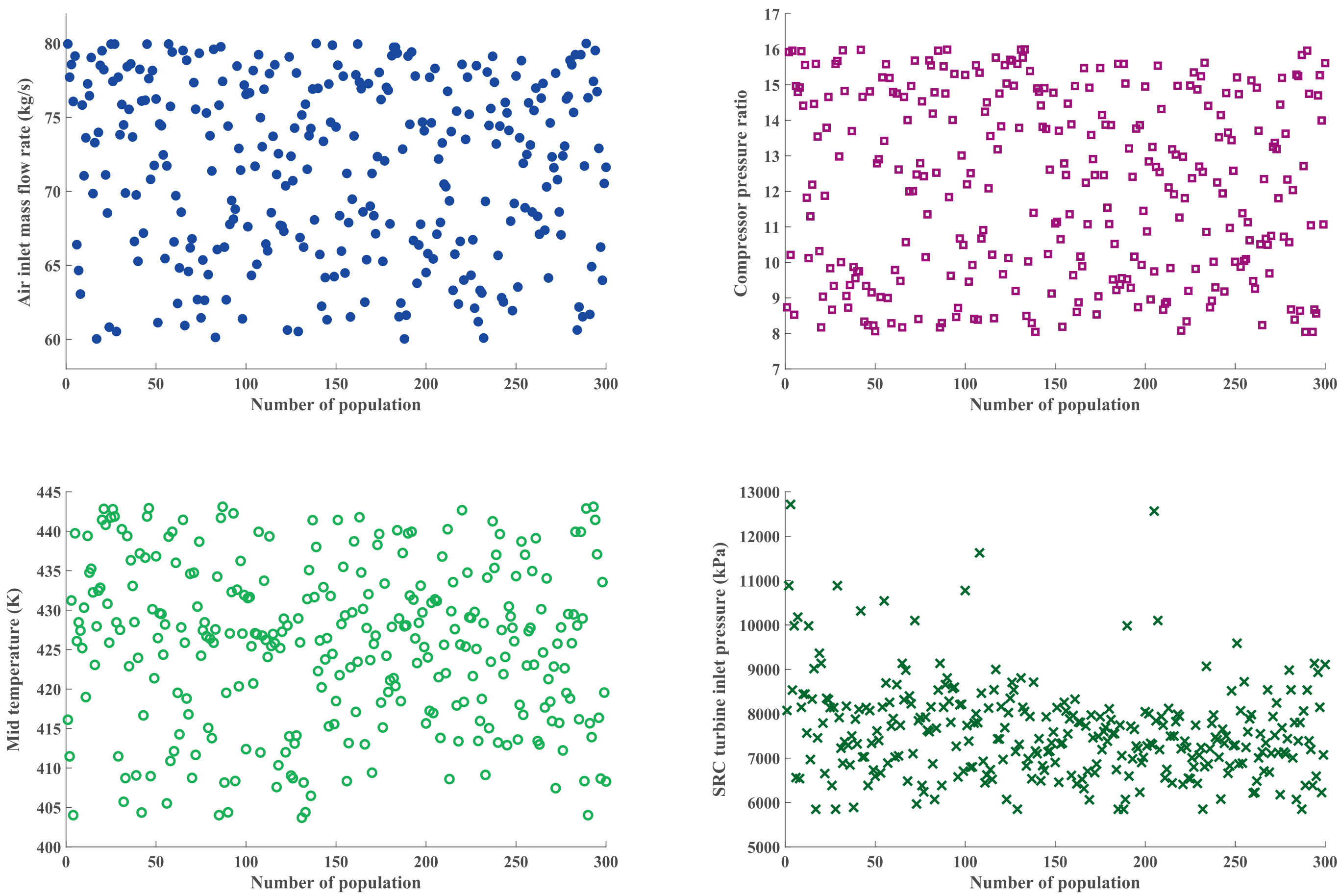

Fig. 8. Population distribution for each decision variable (Without ARC scenario).

- **Membrane Separation (Direct Capture):** After the exhaust gases pass through the thermal recovery stages, the CO_2 separation unit physically filters the flue gas. The separator can capture approximately one-third of the CO_2 generated during the process.
- **Efficiency Gains:** The integration of the bottoming Steam Rankine Cycle (SRC) and low-grade heat recovery via TEGs increases the total net power to 35,483 kW, thereby reducing the specific CO_2 emissions per unit of electricity generated compared to a standalone gas turbine.

These combined strategies enable the system to significantly outperform conventional power plants, which emit higher levels of CO_2 because they lack capture units and fuel blending capabilities.

The proposed system offers several advantages, most notably the high exergetic efficiency of 71% achieved through the synergistic integration of hydrogen blending and cascading waste heat recovery. The dual-stage decarbonization strategy—utilizing both pre-combustion H_2 blending and post-combustion membrane separation—represents a robust approach to emissions mitigation. Furthermore, the scenario-based flexibility allows the plant to adapt to varying thermal demands, providing either 24,000 kW of heating or 18,000 kW of cooling.

However, certain disadvantages must be acknowledged. The system's complexity, involving five distinct subsystems, results in a high initial capital cost and an overall cost rate of 2,845 $/h in the optimal heating scenario. Additionally, reliance on a PEM electrolyzer results in a high Levelized Cost of Hydrogen (1.8–3.5 $/kg) and increases the system's sensitivity to electricity price fluctuations. Finally, the current steady-state model does not account for the challenges of part-load controllability and component degradation over time as provided in Table 11.

5. Conclusion

This research proposed and evaluated an integrated multigeneration energy framework that combines power generation, hydrogen production, and carbon capture within a unified thermodynamic and economic framework. Two operational scenarios were examined: one featuring an absorption refrigeration cycle (ARC) to produce cooling, and another without ARC that channels thermal energy toward heating and enhanced hydrogen output. A comprehensive thermodynamic model, validated against existing studies, was established to replicate the system's behavior. A genetic algorithm coupled with a neural network surrogate model was used to optimize operating conditions for CO_2 reduction, overall cost rate, and exergetic efficacy.

The findings demonstrate that increasing the air mass flow rate to the gas turbine significantly improves power generation and hydrogen production while maintaining exergy efficiency, as reflected in proportional increases in input and output exergy. Varying the compressor pressure ratio enhances thermodynamic performance but reduces hydrogen output and CO_2 reduction. Similarly, increasing the Rankine cycle's turbine inlet pressure promotes hydrogen production and lowers emissions, while higher temperature differentials in the heat exchanger-separator interface result in greater energy losses, reducing overall system performance.

At the optimal point, the scenario without ARC achieved an exergetic efficiency of 71% and a CO_2 reduction rate of 3.9%, though it incurred a slightly higher total cost rate. Conversely, the ARC-equipped scenario offered valuable cooling capacity and a lower LCOE, but at the cost of reduced hydrogen production. Compared to a standalone gas turbine system, both configurations demonstrated significant improvements in energy utilization and emissions mitigation, with the integrated CO_2

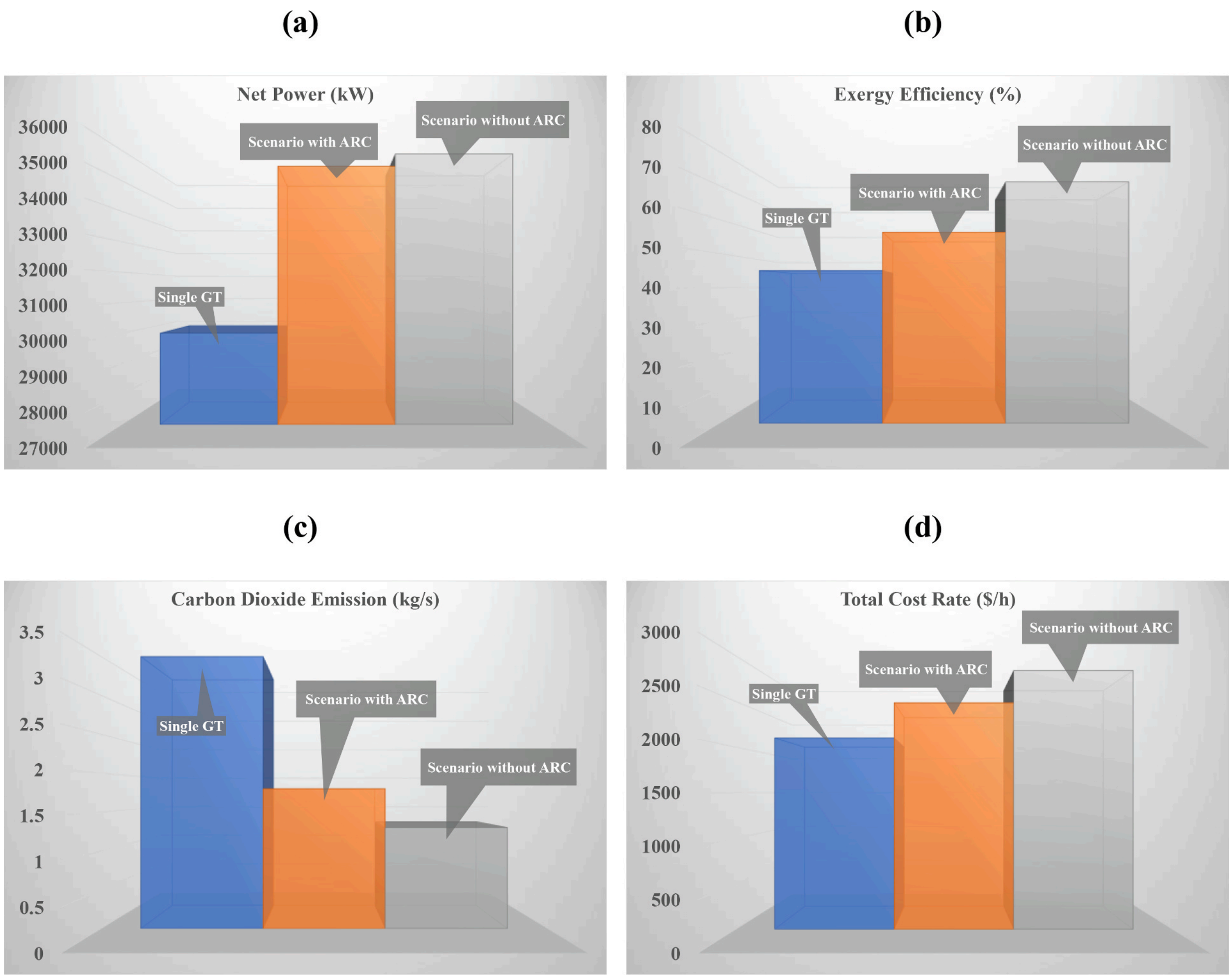

Fig. 9. Comparison between the main outputs of a single GT, scenario A, and scenario B.

Table 10
Exergy destruction at different components.

Component	Exergy destruction for each component (kW)
Air compressor	4200
Combustion chamber	13,600
Gas turbine	3900
Heat exchanger/SRC Evaporator	2600
SRC turbine	1500
SRC condenser	1400
SRC pump	800
Steam generator	3000
Absorber	1000
ARC condenser	850
ARC evaporator	760
Refrigerant expansion valve	200
Solution expansion valve	230
Solution pump	430

capture and hydrogen blending strategies contributing to over 60% reduction in net carbon footprint.

Overall, this work demonstrates the technical and environmental viability of a modular, multi-output energy system that can be tailored to varying thermal demands and decarbonization targets. The proposed architecture offers a pathway toward cleaner distributed energy solutions and can be adapted for diverse applications in urban, industrial, and grid-interactive settings. Future work will explore dynamic operation under variable load conditions and the integration of renewable energy sources to further enhance system flexibility and sustainability.

The proposed integrated multigeneration framework is highly applicable to decentralized energy hubs and industrial complexes seeking to transition toward net-zero operations. Due to its modular design, the system is particularly well-suited for:

- Industrial Districts: Where high-grade electricity can power manufacturing while the 18,000 kW cooling load or 24,000 kW heating load meets process-specific thermal requirements.
- Remote or Islanded Grids: Where on-site hydrogen production (150 kg/h) provides critical energy storage and fuel flexibility, reducing reliance on imported fossil fuels.
- Urban CCHP Hubs: Where the membrane-based CO_2 separation unit can be utilized to meet stringent municipal emission standards while providing district heating or cooling.

These diverse application scenarios demonstrate the system's

Table 11
Comparison between current study results and several studies in the literature [6,22,48].

Study	System Configuration	η_{ex} (%)	CO_2 Reduction	Main Product(s)
Maheshwari et al.	GT + SRC + ORC	57.87	–	Power
Mahmoodi et al.	CCHP + Greenhouse	–	✓	Power, Cooling, CO_2
Yari	Geothermal RC	49.06	–	Power
Present Study	GT + SRC + ARC + PEME + SEP	71	3.90%	Power, H_2, Cooling, CO_2

potential as a scalable solution for sustainable, distributed energy generation.

While the current study establishes a robust theoretical and technical framework for the integrated multigeneration system, it serves as a critical baseline for further practical validation. Future research will focus on addressing operational feasibility through dynamic simulation to evaluate system behavior under transient load conditions. Additionally, experimental pilot-scale studies are necessary to validate the long-term durability of the CO_2 separation membranes and the PEM electrolyzer under a hydrogen-blended fuel environment. Further optimization could also incorporate renewable energy sources, such as solar or wind, to enhance system flexibility and accelerate the transition toward a net-zero energy infrastructure.

CRediT authorship contribution statement

Amr S. Abouzied: Writing – review & editing, Writing – original draft, Supervision, Resources. **Hyder H. Abed Balla:** Investigation, Formal analysis. **Omar J. Alkhatib:** Supervision, Methodology, Conceptualization. **Ahmed G. Abokhalil:** Data curation, Conceptualization. **Mahidzal Dahari:** Validation, Investigation, Funding acquisition, Formal analysis. **M.A. Ahmed:** Writing – original draft, Formal analysis. **Zahra Bayhan:** Writing – review & editing, Resources, Investigation. **Dhaffaf Saud Alrasheed:** Formal analysis, Data curation. **Yasser Fouad:** Writing – review & editing, Writing – original draft, Supervision, Methodology, Funding acquisition. **Ibrahim Mahariq:** Writing – review & editing, Supervision, Resources, Investigation, Formal analysis.

Declaration of competing interest

The authors declare that they have no known competing financial interests or personal relationships that could have appeared to influence the work reported in this paper.

Acknowledgement

Ongoing Research Funding program, (ORF-2026-698), King Saud University, Riyadh, Saudi Arabia.

Data availability

The authors do not have permission to share data.

References

[1] Liu L, Xu Z, Wang L, Wang Y, Li H, Wu Y. Theoretical analysis on high-efficiency combustion and emissions reduction strategy of ammonia-diesel direct injection marine medium-speed engines under energizing-intensifying composite combustion mode. Appl Therm Eng 2025;278:127391. https://doi.org/10.1016/j.applthermaleng.2025.127391.

[2] He Q, Qu C. Waste-to-energy-coupled AI data centers: Cooling efficiency and grid resilience. arXiv 2025;2512.24683, doi: 10.48550/arXiv.2512.24683.

[3] Liu S, Fan F, Wang A, Xu W, Zhao L, Chen R. 3D simulation and performance analysis of the non-isothermal charge/discharge processes in thermo-electrochemical cycle. J Power Sources 2026;661:238695. https://doi.org/10.1016/j.jpowsour.2025.238695.

[4] Li J, Chen X, Shen J, Zhang Y, Liu D. Optimal heat storage temperature and performance of ORC-based Carnot battery at various application scenarios. Energy Convers Manag 2024;318:118906. https://doi.org/10.1016/j.enconman.2024.118906.

[5] Wang H, Yi Z, Xu Y, Xie Y, Li Z. Integrating virtual heat plants into combined heat and power system dispatch: a new pathway to improve the air quality. Sustain Energy Grids Netw 2026;46:102151. https://doi.org/10.1016/j.segan.2026.102151.

[6] Nasrabadi AM, Malaei O, Moghimi M, Sadeghi S. Deep learning optimization of a combined CCHP and greenhouse for CO 2 capturing ; case study of Tehran Coefficient of Perfor. Energy Convers Manag 2022;267:115946. https://doi.org/10.1016/j.enconman.2022.115946.

[7] Jiang Y, Wang J, Zhao H, Terzija V. Dynamic interval state estimation for integrated electricity and heating systems. IEEE Trans Power Syst 2026;41:82–95. https://doi.org/10.1109/TPWRS.2025.3600251.

[8] Haghghi MA, Feili M, Nourani P, Bahman AM. An intelligent NSGA-II-based optimization of a novel biogas-fed oxyfuel gas turbine cycle using CO2 capture option coupled with a multi-heat recovery network and a multi-effect desalination cycle. Desalination 2025;612:118957. https://doi.org/10.1016/j.desal.2025.118957.

[9] Wan A, Xiong Z, Al-Bukhaiti K, Yin R, Yuan J, Cheng X, et al. An integrated TCN-ECA-BiLSTM and TD3 framework for high-accuracy forecasting and optimal load allocation in combined heat and power systems. Energy 2026;350:140670. https://doi.org/10.1016/j.energy.2026.140670.

[10] Feili M, Ghaebi H, Haghghi MA. Data-driven optimization of an innovative environmentally friendly power-methanol co-production system utilizing biogas-driven S-Graz cycle, biogas steam reforming, and CO2 capture-hydrogenation process. Renew Energy 2025;255:123835. https://doi.org/10.1016/j.renene.2025.123835.

[11] Wilberforce T, Olabi AG, Sayed ET, Elsaid K, Abdelkareem MA. Progress in carbon capture technologies. Sci Total Environ 2021;761:143203. https://doi.org/10.1016/j.scitotenv.2020.143203.

[12] Nanzeeba F, Baigh TA, Kabir A, Khan Y, Ehsan MM. Genetic algorithm-based optimization of combined supercritical CO2 power and flash-tank enhanced transcritical CO2 refrigeration cycle for shipboard waste heat recuperation. Energy Rep 2024;12:1810–35. https://doi.org/10.1016/j.egyr.2024.07.059.

[13] Feili M, Nourani P, Haghghi MA, Bahman AM. Machine learning optimization of integrating an advanced thermal-electrochemical plant with an oxy-biogas fuel plant employing a CO2 capture process. Energy Convers Manag 2025;335:119871. https://doi.org/10.1016/j.enconman.2025.119871.

[14] Jarvis SM, Samsatli S. Technologies and infrastructures underpinning future CO2 value chains: a comprehensive review and comparative analysis. Renew Sustain Energy Rev 2018;85:46–68. https://doi.org/10.1016/j.rser.2018.01.007.

[15] Sadman Bishal S, Imtiaz Anando A, Fahim Faysal D, Monjurul EM. Performance evaluation of a novel multigeneration plant of cooling, power, and seawater desalination using Supercritical CO2 partial cooling, ME-TVC desalination, and absorption refrigeration cycles. Energy Convers Manag X 2023;20:100485. https://doi.org/10.1016/j.ecmx.2023.100485.

[16] Guillermo Garcia-Garcia, Marta Cruz Fernandez, Katy Armstrong, Steven Woolas PS. ChemSusChem - 2020 - Garcia-Garcia - Analytical Review of Life-Cycle Environmental Impacts of Carbon Capture and.pdf n.d.

[17] Ghiat I, Al-Ansari T. A review of carbon capture and utilisation as a CO2abatement opportunity within the EWF nexus. J CO2 Util 2021;45:101432. https://doi.org/10.1016/j.jcou.2020.101432.

[18] Baigh TA, Saif MJ, Mustakim A, Nanzeeba F, Khan Y, Ehsan MM. Enhancing thermodynamic performance with an advanced combined power and refrigeration cycle with dual LNG cold energy utilization. Heliyon 2024;10:e35748. https://doi.org/10.1016/j.heliyon.2024.e35748.

[19] Rinik RA, Islam N, Ehsan MM, Khan Y. Design of gravity assisted heat exchanger and its application on enhanced waste heat recuperation utilizing organic Rankine and LNG system. Int J Thermofluids 2024;24:100822. https://doi.org/10.1016/j.ijft.2024.100822.

[20] Bishal SS, Faysal DF, Ehsan MM, Salehin S. Performance evaluation of an integrated cooling and power system combining supercritical CO2, gas turbine, absorption refrigeration, and organic rankine cycles for waste energy recuperating system. Results Eng 2023;17:100943. https://doi.org/10.1016/j.rineng.2023.100943.

[21] Olumayegun O, Wang M, Kelsall G. Closed-cycle gas turbine for power generation: a state-of-the-art review. Fuel 2016;180:694–717. https://doi.org/10.1016/j.fuel.2016.04.074.

[22] Maheshwari M, Singh O. Comparative evaluation of different combined cycle configurations having simple gas turbine, steam turbine and ammonia water turbine. Energy 2019;168:1217–36. https://doi.org/10.1016/j.energy.2018.12.008.

[23] Zhong Z, Huo Z, Wang X, Liu F, Pan Y. New steam turbine operational mode for a gas turbine combine cycle bottoming cycle system. Appl Therm Eng 2021;198:117451. https://doi.org/10.1016/j.applthermaleng.2021.117451.

[24] Xiao G, Chen J, Ni M, Cen K. A solar micro gas turbine system combined with steam injection and ORC bottoming cycle. Energy Convers Manag 2021;243:114032. https://doi.org/10.1016/j.enconman.2021.114032.

[25] Lu N, Pan L, Liu Z, Lee KY, Song Y, Si P. Dynamic modeling of thermal-supply system for two-by-one combined-cycle gas and steam turbine unit. Fuel Process Technol 2020;209:106549. https://doi.org/10.1016/j.fuproc.2020.106549.

[26] Laleh SS, Rezaei Mousavi HS, Rabet S, Nojavan F, Yari M, Soltani S. Solar thermal assisted proton exchange membrane electrolyzer and solid oxide fuel cell system based on biomass gasification for green power and hydrogen production: multi-objective optimization and exergoeconomic analysis. Energy Convers Manag 2025;337:119900. https://doi.org/10.1016/j.enconman.2025.119900.

[27] Rabet S, Mahmoudi SMS, Yari M, Soltani S. Dual-combustion chamber cycle utilizing biomass and geothermal energy: a comprehensive economic analysis and multi-objective optimization for enhanced multi-generation. Renew Energy 2025;244:122760. https://doi.org/10.1016/j.renene.2025.122760.

[28] Oymak BA, Yilmaz F. Development of a novel integrated energy system based on waste heat recovery for sustainable products: a thermodynamic assessment. Therm Sci Eng Prog 2025;64:103806. https://doi.org/10.1016/j.tsep.2025.103806.

[29] Cao Y, Mohamed AM, Dahari M, Delpisheh M, Haghghi MA. Performance enhancement and multi-objective optimization of a solar-driven setup with storage process using an innovative modification. J Storage Mater 2020;32:101956. https://doi.org/10.1016/j.est.2020.101956.

[30] Besagni G, Mereu R, Inzoli F. Ejector refrigeration: a comprehensive review. Renew Sustain Energy Rev 2016;53:373–407. https://doi.org/10.1016/j.rser.2015.08.059.
[31] Khan TE, Sakib SH, Sakib N, Hossain T, Ehsan MM, Khan Y. Multi-Objective optimization of a cascaded supercritical CO2 brayton cycle with ejector-enhanced transcritical CO2 and flash tank absorption refrigeration cycles. Energy Convers Manag X 2025;26:100988. https://doi.org/10.1016/j.ecmx.2025.100988.
[32] Ahmed MM, Bishal SS, Ehsan MM, Khan Y. Multi-effect distillation with novel liquid vapor ejector utilizing the waste heat from intercoolers of a single mixed refrigerant cycle for natural gas liquefaction. Clean Energy Syst 2025;10:100182. https://doi.org/10.1016/j.cles.2025.100182.
[33] Khan JUR, Zubair SM. Design and rating of an integrated mechanical-subcooling vapor-compression refrigeration system. Energy Convers Manag 2000;41:1201–22. https://doi.org/10.1016/S0196-8904(99)00169-7.
[34] Ahamed JU, Saidur R, Masjuki HH. A review on exergy analysis of vapor compression refrigeration system. Renew Sustain Energy Rev 2011;15:1593–600. https://doi.org/10.1016/j.rser.2010.11.039.
[35] Papadopoulos AI, Kyriakides AS, Seferlis P, Hassan I. Absorption refrigeration processes with organic working fluid mixtures- a review. Renew Sustain Energy Rev 2019;109:239–70. https://doi.org/10.1016/j.rser.2019.04.016.
[36] Moghimi M, Emadi M, Ahmadi P, Moghadasi H. 4E analysis and multi-objective optimization of a CCHP cycle based on gas turbine and ejector refrigeration. Appl Therm Eng 2018;141:516–30. https://doi.org/10.1016/j.applthermaleng.2018.05.075.
[37] Abbasi M, Chahartaghi M, Hashemian SM. Energy, exergy, and economic evaluations of a CCHP system by using the internal combustion engines and gas turbine as prime movers. Energy Convers Manag 2018;173:359–74. https://doi.org/10.1016/j.enconman.2018.07.095.
[38] Chen WD, Chua KJ. Energy performance analysis and optimization of a coupled adsorption and absorption cascade refrigeration system. Appl Energy 2021;301:117518. https://doi.org/10.1016/J.APENERGY.2021.117518.
[39] Li G, Xu J, Liu S, Zhao D, Zheng Y, Guo W. High-energy density micro swirl combustion powered thermoelectric generator for combined heat and power supply. Therm Sci Eng Prog 2025;68:104369. https://doi.org/10.1016/j.tsep.2025.104369.
[40] Arashrad P, Sharafi Laleh S, Rabet S, Yari M, Soltani S, Rosen MA. Real-time modeling of a solar-driven power plant with green hydrogen, electricity, and fresh water production: techno-economics and optimization. Sustainability 2025;17. https://doi.org/10.3390/su17083555.
[41] Rabet S, Laleh SS, Habibi O, Sadri Jahanshahi SA, Yari M, Soltani S. A novel multi-generation system integrating thermophotovoltaic and SOFC system for power and green hydrogen with CO2 liquefaction: a techno-economic and multi-objective optimization study. Fuel 2026;405:136581. https://doi.org/10.1016/j.fuel.2025.136581.
[42] Chitsaz A, Haghghi MA, Hosseinpour J. Thermodynamic and exergoeconomic analyses of a proton exchange membrane fuel cell (PEMFC) system and the feasibility evaluation of integrating with a proton exchange membrane electrolyzer (PEME). Energy Convers Manag 2019;186:487–99. https://doi.org/10.1016/j.enconman.2019.03.004.
[43] Taamallah S, Vogiatzaki K, Alzahrani FM, Mokheimer EMA, Habib MA, Ghoniem AF. Fuel flexibility, stability and emissions in premixed hydrogen-rich gas turbine combustion: technology, fundamentals, and numerical simulations. Appl Energy 2015;154:1020–47. https://doi.org/10.1016/j.apenergy.2015.04.044.
[44] Meziane S, Bentebbiche A. Numerical study of blended fuel natural gas-hydrogen combustion in rich/quench/lean combustor of a micro gas turbine. Int J Hydrogen Energy 2019;44:15610–21. https://doi.org/10.1016/j.ijhydene.2019.04.128.
[45] Ozturk M, Dincer I. Development of a combined flash and binary geothermal system integrated with hydrogen production for blending into natural gas in daily applications. Energy Convers Manag 2021;227:113501. https://doi.org/10.1016/j.enconman.2020.113501.
[46] Pourrahmani H, Moghimi M. Exergoeconomic analysis and multi-objective optimization of a novel continuous solar-driven hydrogen production system assisted by phase change material thermal storage system. Energy 2019;189:116170. https://doi.org/10.1016/j.energy.2019.116170.
[47] Raiyan AR, Samiuzzaman KY, Ehsan MM, Karim MR, Siddique SM. Exergoeconomic analysis and multi objective optimization of a nuclear driven integrated cooling and power cycle using response surface regression modeling coupled with genetic algorithm. Energy Convers Manag 2025;337:119836. https://doi.org/10.1016/j.enconman.2025.119836.
[48] Sharafi Laleh S, Rabet S, Rezaei Mousavi HS, Yari M, Soltani S, Saberi MA. Techno-economic optimization of an integrated ammonia–methane synthesis system powered by LNG-assisted biogas oxy-fuel cycle and vanadium chloride hydrogen production. Energy 2025;336:138380. https://doi.org/10.1016/j.energy.2025.138380.
[49] Adebayo V, Abid M, Adedeji M, Hussain Ratlamwala TA. Energy, exergy and exergo-environmental impact assessment of a solid oxide fuel cell coupled with absorption chiller & cascaded closed loop ORC for multi-generation. Int J Hydrogen Energy 2022;47:3248–65. https://doi.org/10.1016/j.ijhydene.2021.02.222.
[50] Compernolle T, Witters N, Van Passel S, Thewys T. Analyzing a self-managed CHP system for greenhouse cultivation as a profitable way to reduce CO2-emissions. Energy 2011;36:1940–7. https://doi.org/10.1016/j.energy.2010.02.045.
[51] Campanari S, Chiesa P, Manzolini G, Bedogni S. Economic analysis of CO2 capture from natural gas combined cycles using Molten Carbonate fuel Cells. Appl Energy 2014;130:562–73. https://doi.org/10.1016/j.apenergy.2014.04.011.
[52] Nami H, Akrami E, Ranjbar F. Hydrogen production using the waste heat of Benchmark pressurized Molten carbonate fuel cell system via combination of organic Rankine cycle and proton exchange membrane (PEM) electrolysis. Appl Therm Eng 2017;114:631–8. https://doi.org/10.1016/j.applthermaleng.2016.12.018.
[53] Zang G, Jia J, Tejasvi S, Ratner A, Silva LE. Techno-economic comparative analysis of Biomass Integrated Gasification combined Cycles with and without CO2 capture. Int J Greenh Gas Control 2018;78:73–84. https://doi.org/10.1016/j.ijggc.2018.07.023.
[54] Wu Z, Zhu P, Yao J, Zhang S, Ren J, Yang F, et al. Combined biomass gasification, SOFC, IC engine, and waste heat recovery system for power and heat generation: Energy, exergy, exergoeconomic, environmental (4E) evaluations. Appl Energy 2020;279:115794. https://doi.org/10.1016/j.apenergy.2020.115794.
[55] Zhu Y, Li W, Li J, Li H, Wang Y, Li S. Thermodynamic analysis and economic assessment of biomass-fired organic Rankine cycle combined heat and power system integrated with CO2 capture. Energy Convers Manag 2020;204:112310. https://doi.org/10.1016/j.enconman.2019.112310.
[56] Bejan A, Tsatsaronis G, Moran MJ. Thermal design and optimization. John Wiley & Sons, Ltd; 1995.
[57] Mehrenjani JR, Gharehghani A, Nasrabadi AM, Moghimi M. Design, modeling and optimization of a renewable-based system for power generation and hydrogen production. Int J Hydrogen Energy 2022;47:14225–42. https://doi.org/10.1016/j.ijhydene.2022.02.148.
[58] Falcão DS, Pinto AMFR. A review on PEM electrolyzer modelling: guidelines for beginners. J Clean Prod 2020;261:121184. https://doi.org/10.1016/J.JCLEPRO.2020.121184.
[59] Asadbagi P, Nasrabadi AM, Hall CM. Full analysis and deep learning optimization of a sustainable and eco-friendly power plant to generate green hydrogen and electricity; a zero-carbon approach. Process Saf Environ Prot 2024;190:277–97. https://doi.org/10.1016/j.psep.2024.07.029.
[60] Chitgar N, Emadi MA, Chitsaz A, Rosen MA. Investigation of a novel multigeneration system driven by a SOFC for electricity and fresh water production. Energy Convers Manag 2019;196:296–310. https://doi.org/10.1016/j.enconman.2019.06.006.
[61] Chitgar N, Moghimi M. Design and evaluation of a novel multi-generation system based on SOFC-GT for electricity, fresh water and hydrogen production. Energy 2020;197:117162. https://doi.org/10.1016/j.energy.2020.117162.
[62] Zhao L, Riensche E, Blum L, Stolten D. Multi-stage gas separation membrane processes used in post-combustion capture: energetic and economic analyses. J Memb Sci 2010;359:160–72. https://doi.org/10.1016/J.MEMSCI.2010.02.003.
[63] Yuan M, Teichgraeber H, Wilcox J, Brandt AR. Design and operations optimization of membrane-based flexible carbon capture. Int J Greenh Gas Control 2019;84:154–63. https://doi.org/10.1016/j.ijggc.2019.03.018.
[64] Merkel TC, Lin H, Wei X, Baker R. Power plant post-combustion carbon dioxide capture: an opportunity for membranes. J Memb Sci 2010;359:126–39. https://doi.org/10.1016/J.MEMSCI.2009.10.041.
[65] Qiao T, Li W, Liu W, Xu G, Jin H. Design considerations and many-objective optimization of synchronous condenser used for new energy power system based on electromagnetic-thermal constraints. IEEE Trans Ind Electron 2025:1–12. https://doi.org/10.1109/TIE.2025.3637402.
[66] Zhang Y, Li J, Yu M, Chen X, Chen X, Shen J. Dominant factor identification and fast optimization of Carnot battery by integrating SHAP and physics-guided neural network. Appl Energy 2025;401:126641. https://doi.org/10.1016/j.apenergy.2025.126641.
[67] Mehrenjani JR, Gharehghani A, Sangesaraki AG. Machine learning optimization of a novel geothermal driven system with LNG heat sink for hydrogen production and liquefaction. Energy Convers Manag 2022;254:115266. https://doi.org/10.1016/j.enconman.2022.115266.
[68] Yari M. Exergetic analysis of various types of geothermal power plants. Renew Energy 2010;35:112–21. https://doi.org/10.1016/j.renene.2009.07.023.